Article:

Zhuang, P-Z orcid.org/0000-0002-7377-7297, Yu, H-S and Hu, N (2018) Size-dependent finite strain analysis of cavity expansion in frictional materials. International Journal of Solids and Structures, 150. pp. 282-294. ISSN 0020-7683

https://doi.org/10.1016/j.ijsolstr.2018.06.023

Size-dependent finite strain analysis of cavity expansion in frictional materials

Pei-Zhi Zhuang, Hai-Sui Yu , Nian Hu*

ABSTRACT: This paper presents unified solutions for elastic-plastic expansion analysis of a cylindrical or spherical cavity in an infinite medium, adopting a flow theory of strain gradient plasticity. Previous cavity expansion analyses incorporating strain gradient effects have mostly focused on explaining the strain localisation phenomenon and/or size effects during infinitesimal expansions. This paper is however concerned with the size-dependent behaviour of a cavity during finite quasi-static expansions. To account for the non-local influence of underlying microstructures to the macroscopic behaviour of granular materials, the conventional Mohr-Coulomb yield criterion is modified by including a second-order strain gradient. Thus the quasi-static cavity expansion problem is converted into a second-order ordinary differential equation system. In the continuous cavity expansion analysis, the resulting governing equations are solved numerically with Cauchy boundary conditions by simple iterations. Furthermore, a simplified method without iterations is proposed for calculating the size-dependent limit pressure of a cavity expanding to a given final radius. By neglecting the elastic strain increments in the plastic zone, approximate analytical size-dependent solutions are also derived. It is shown that the strain gradient effect mainly concentrates in a close vicinity of the inner cavity. Evident size-strengthening effects associated with the sand particle size and the cavity radius in the localised deformation zone are captured by the newly developed solutions presented in this paper. The strain gradient effect will vanish when the intrinsic material length is negligible compared to the instantaneous cavity size, and then the conventional elastic perfectly-plastic solutions can be recovered exactly. The present solutions can provide a theoretical method for modelling the size effect that is often observed in small sized sand-structure interaction problems.

Keywords: Cavity expansion, Strain gradient plasticity, Size effect, Finite strain, Quasi-static analysis

1. Introduction

Cavity expansion theory is a specific theoretical approach to study the evolution of stress and deformation fields associated with an expanding cavity. It has been first developed for applications to metal indentation problems (Bishop et al., 1945) and has attracted much attention afterwards due to its successful applications to a wide range of engineering problems (Hill, 1950; Yu, 2000). In particular, cavity expansion solutions provide a useful and simple theoretical tool in the analysis and design of a variety of practical geotechnical problems, such as interpretations of in situ soil testing (e.g., pressuremeter tests (PMTs), cone penetration tests (CPTs)) and bearing capacity predictions of pile foundations and earth anchors (Hughes et al., 1977; Randolph et al., 1994; Yu, 2000, 2006). By using more and more realistic soil constitutive models, significant progress has been made over the past several decades in developing accurate cavity expansion solutions for both sand and clay (Chadwick, 1959; Collins and Yu, 1996; Gibson and Anderson, 1961; Mo and Yu, 2016; Russell and Khalili, 2006; Salgado et al., 1997; Yu and Houlsby, 1991). As the soil constitutive models have been mostly established within the context of conventional continuum theory, potential influences of microstructures (or soil fabric) to the macroscopic behaviour and properties of granular soils unfortunately have been neglected in previous cavity expansion solutions. In fact, microstructures (e.g., irregular grains, micro pores, and micro cracks) widely exist in granular materials and may apply significant influences on the overall macroscopic response of the material under some circumstances as discussed below. Aiming to additionally consider the microstructural effect in the quasi-static cavity expansion analysis in frictional material, this paper presents unified finite expansion solutions for both cylindrical and spherical cavities by adopting a simple flow theory of strain gradient plasticity. First of all, relevant developments on this topic are briefly reviewed.

Experimental evidence is accruing for the existence of a strong size-dependent strengthening effect in many interaction problems between geotechnical structures and geomaterials. It is generally observed that the smaller the structure size is, the stiffer soil response may be experienced. For example, greater tip resistances are often measured by smaller penetrometers in CPTs (Balachowski, 2007; Bolton et al., 1999; De Beer, 1963; Eid, 1987; Lima and Tumay, 1991; Wu and Ladjal, 2014), the shaft friction and toe resistance of piles tend to increase with decreases of the pile diameter (Balachowski, 2006; Chow, 1996; Lehane et al., 2005; Meyerhof, 1983; Turner and Kulhawy, 1994; Wernick, 1978), the normalised uplift bearing factor of earth anchors may increase with an decreasing ratio of anchor-to-soil grain size

(Athani et al., 2017; Sakai et al., 1998; Tagaya et al., 1988). In general, it is found that the size effects existing in these non-dimensional results of the soil resistance closely relate to the ratio of the structure size over the grain size. While the structure size or the dominant plastic deformation becomes comparable to the intrinsic material length scales, it has been suggested that the size-dependent material response may stem from the interaction between the geometric size of the structure/externally applied loads and intrinsic material lengths/internal forces associated with the underlying microstructures (Aifantis, 1999). The interaction between the macroscopic and microscopic length scales are now generally modelled by introducing extra higher-order deformation gradients into the constitutive models or considering additional degrees of freedom, and thus high-order theories of elasticity and plasticity with inclusions of different intrinsic material lengths have been developed (Aifantis, 1987, 2003; Fleck and Hutchinson, 1997; Gao et al., 1999; Gudmundson, 2004; Huang et al., 2004; Hutchinson, 2012; Mindlin, 1964; Mühlhaus and Aifantis, 1991; Toupin, 1962; Zhao et al., 2005; Zhou et al., 2002). Among them, the strain gradient plasticity theories proposed by Aifantis and his co-workers (Al Hattamleh et al., 2004; De Borst and Mühlhaus, 1992; Mühlhaus and Aifantis, 1991; Vardoulakis and Aifantis, 1989, 1991; Zbib and Aifantis, 1989; Zervos et al., 2001) have been successfully applied in a variety of strain localisation and instability analyses of geomaterials. Within this framework, a simple flow theory of strain gradient plasticity for frictional materials like sand is developed first by incorporating a second-order strain gradient into the Mohr-Coulomb yield function, and then it is applied to the quasi-static cavity expansion analysis in order to capture the commonly observed size-strengthening effects associated with the cavity/structure size and the particle size in the many geotechnical applications of the cavity expansion theory.

Note that there have been a number of early works studying on the size effect and/or deformation localisation phenomenon around a cavity using higher-order theories. Based on strain gradient elasticity theories, some analytical elastic solutions have been developed, for example, Aifantis (1996); Collin et al. (2009); Eshel and Rosenfeld (1970). As far as plastic yielding of the material is concerned, some elastic-plastic cavity solutions have also been proposed. For example, based on deformation-version of strain gradient plasticity models incorporating the Laplacian of the effective plastic strain into the constitutive expression of the flow stress, Gao (2002, 2003a, b, 2006) derived analytical solutions for modelling the size effect on the stress and strain distributions around an internally pressurized thick-walled cylinder or spherical shell of different hardening materials. Similar problems around a thick-walled hollow cylinder were further investigated by Tsagrakis et al. (2004) using both deformation version and flow version of gradient plasticity theories. Subsequently, by using a wavelet-based scale-dependent model, Tsagrakis et al. (2006) presented an analytical solution for the same problem with a consideration of the size effect. Unfortunately, the constitutive relations adopted in these solutions are not generally suitable for characterising the behaviour of geomaterials, and assumptions on the infinitesimal deformation and/or incompressibility of materials further restrict their applications to the geotechnical problems with large deformations. For granular materials, by additionally considering strain gradients and their work-conjugate forces in the expressions of strains and stresses, Zhao et al. (2007) presented a numerical solution for the elastic-plastic analysis of a pressurised cylinder of a modified Tresca-type material. Subsequently, Zhao (2011) extended the solution to cohesive-frictional materials for both cylindrical and spherical cavities. The size-dependent elastic-plastic soil responses during infinitesimal cavity expansions have been studied therein. By neglecting the elastic strains in the plastic region, Ladjal (2013) derived two approximate spherical cavity expansion solutions with different inclusion methods of the second-order strain gradient into the Drucker-Prager yield criterion. As the small strain assumption has also been adopted, these solutions are not capable of modelling the size-dependent continuous cavity expansion problem with large deformations either. Overall, previous solutions based on non-local theories mainly focused on the size effect and/or stress concentration/strain localisation problems in the static analysis or at infinitesimal deformations. The size-dependent behaviour in quasi-static finite cavity expansions has seldom been studied so far. Therefore, by adopting the proposed strain gradient plasticity model for granular materials, size-dependent (or strain-gradient-dependent) finite strain solutions for quasi-static expansion analysis of both cylindrical and spherical cavities are developed in this paper.

2. Problem definition and strain gradient plasticity model

A cylindrical/spherical cavity is expanded by a uniformly distributed internal pressure p within an infinite medium of sand. Initially the cavity radius is a_0 and a hydrostatic pressure p_0 acts throughout the soil (e.g., Fig. 1). With an increasing internal compression pressure from p_0 to p, the cavity expands outwards monotonically from a_0 to a with a sufficiently slow speed. For convenience, cylindrical coordinates (r, θ, z) and spherical coordinates (r, θ, φ) with the origin located in the centre of the cavity are employed to describe the spatial locations of points in the expansion process of a cylindrical and spherical cavity respectively. The cylindrical cavity expansion analysis is conducted under plane strain condition with respect to the z-axis. Then the stress equilibrium condition in the radial direction during a symmetrical expansion is readily expressed as

$$\sigma_\theta - \sigma_\mathrm{r} = \frac{\mathrm{r}}{\mathrm{k}} \frac{\partial \sigma_\mathrm{r}}{\partial \mathrm{r}} \tag{1}$$

where σ_θ and σ_r represents the circumferential and radial principal stress components respectively. $\mathrm{k} = 1$ for a cylindrical cavity, and $\mathrm{k} = 2$ for a spherical cavity.

'Standard' stress boundary conditions for the defined problem (taking tension as positive) are

$$\sigma_\mathrm{r}\big|_{\mathrm{r}=\mathrm{a}} = -\mathrm{p} \quad , \quad \sigma_\mathrm{r}\big|_{\mathrm{r}\to\infty} = -\mathrm{p}_0 \tag{2 a,b}$$

The surrounding material of the cavity behaves elastically and obeys the Hooke's law until the onset of yielding. Considering the microstructural effect, the plastic response is characterised by a strain gradient plasticity model with reference to the method suggested by Aifantis and his co-workers (Aifantis, 1987; Mühlhaus and Aifantis, 1991; Vardoulakis and Aifantis, 1989; Zbib and Aifantis, 1989). Strain gradients are additionally incorporated into the term of frictional property in the plastic flow stress. The gradient terms represent a macroscopic manifestation of the inhomogeneous evolution of underlying microstructures in a Representative Volume Element (RVE) (Mühlhaus and Aifantis, 1991; Zbib and Aifantis, 1989). With the Taylor series expansion, the cumulative average strain $\bar{\gamma}_\mathrm{p}$ within a symmetric neighbourhood (i.e., RVE) of one local point can be obtained as detailed in the Appendix A. As the contribution of strain gradients higher than the second order was found to be minimal (Al Hattamleh et al., 2004), only the second-order strain gradient is considered here as others, for example, Al Hattamleh et al. (2004); De Borst and Mühlhaus (1992); Vardoulakis and Aifantis (1991). Then $\bar{\gamma}_\mathrm{p}$ can be summarised as

$$\bar{\gamma}_\mathrm{p} = \gamma_\mathrm{p} + \mathrm{C}_\mathrm{nD} \nabla^2 \gamma_\mathrm{p} \tag{3}$$

where the coefficient is $\mathrm{C}_\mathrm{2D} = \mathrm{R}_\mathrm{g}{}^2/8$ for plane problems and $\mathrm{C}_\mathrm{3D} = \mathrm{R}_\mathrm{g}{}^2/10$ for three dimensional problems. ∇^2 is the Laplacian operator. R_g represents the radius of a RVE.

In strain gradient plasticity models for granular soils, high-order strain gradients have often been introduced to modify the flow stress of the yield function (Al Hattamleh et al., 2004; De Borst and Mühlhaus, 1992; Mühlhaus and Aifantis, 1991; Zbib and Aifantis, 1989). Meanwhile, attempts have also been made to modify the plastic flow rule (dilatancy condition)

(Vardoulakis and Aifantis, 1989) or the friction and dilation properties simultaneously in the strain localisation analysis (e.g., shear band) (Vardoulakis and Aifantis, 1991). For frictional materials like sand, in general, the friction angle is significantly strain-dependent (Guo and Stolle, 2005), but it has been suggested that the dilation angle is more likely strain-independent (Bolton, 1986; Chakraborty and Salgado, 2010; Schanz and Vermeer, 1996). According to these characteristics, the second-order strain gradient is only introduced to modify the friction strength of the yield stress in the conventional plasticity theory while remaining the structure of the flow function unaltered. Hence the modified Mohr-Coulomb yield criterion for cohesionless materials goes to

$$\mathrm{f} = \bar{\alpha}\sigma_1 - \sigma_3 \tag{4}$$

where σ_1 and σ_3 are the major and minor principal stress respectively. $\bar{\alpha}$ represents the modified stress flow number associated with the friction angle φ of sand with an inclusion of the Laplacian of equivalent plastic shear strain (γ_{p}) as

$$\bar{\alpha} = \alpha + \mathrm{c_g}\nabla^2\gamma_{\mathrm{p}} \tag{5}$$

where α represents the homogeneous part of the friction strength, namely $\alpha = (1+\sin\varphi)/(1-\sin\varphi)$ keeping consistent with that in the perfectly-plastic model. $\mathrm{c_g}$ is a phenomenological strain gradient coefficient.

It is assumed that the plastic strain rates ($\dot{\varepsilon}_{\mathrm{ij}}^{\mathrm{p}}$) are proportional to $\dot{\gamma}_{\mathrm{p}}$ and the plastic flow directions are determined by the normality condition with respect to the plastic potential function g (Al Hattamleh et al., 2004; Vardoulakis and Aifantis, 1991). Mathematically, it gives

$$\dot{\varepsilon}_{\mathrm{ij}}^{\mathrm{p}} = \frac{\partial \mathrm{g}}{\partial \sigma_{\mathrm{ij}}}\dot{\gamma}_{\mathrm{p}} \tag{6}$$

where $\mathrm{g} = \beta\sigma_1 - \sigma_3$ and $\beta = (1+\sin\psi)/(1-\sin\psi)$ for cohesionless Mohr-Coulomb materials following a non-associated flow rule. ψ is the dilation angle of sand. σ_{ij} represents stress components.

Dimensional analysis shows $\mathrm{c_g}$ has a dimension of $[\mathrm{L}^2]$. Comparing Eqs. (3) and (5), an intrinsic material length representing the statistical scope of the contributing area/volume to the local deformation is incorporated into the gradient plasticity model. The inherent material length (uniformly represented by $\mathrm{l_g}$) of sand is often approximated by its mean particle size (i.e., $l_g \approx d_{50}$) (Al Hattamleh et al., 2004; Vardoulakis and Aifantis, 1991). In addition, it has been suggested that c_g also includes a dimensionless modulus-like index (H_g) regulating the magnitude of the gradient effect (Mühlhaus and Aifantis, 1991; Vardoulakis and Aifantis, 1991). Physically H_g represents the dependency of $\bar{\alpha}$ on the variation of $\nabla^2(\gamma_p)$. For modelling the commonly observed size-strengthening effect as introduced previously, the sign of c_g is taken as positive here. Due to the lack of sufficient experimental data, H_g is often assumed as a constant value associated with the normalised elastic shear modulus for simplicity (De Borst and Mühlhaus, 1992; Gao, 2002; Ladjal, 2013; Tsagrakis et al., 2004; Zbib, 1994). Taking above into consideration, the phenomenological strain gradient coefficient c_g in Eq.(5) is expressed as

$$c_g = \rho(G / \sigma_{atm}) {d_{50}}^2 \tag{7}$$

where G is the elastic shear modulus of sand, which depends on the confining pressure level and packing conditions of sand particles (Mitchell and Soga, 2005). The soil elastic stiffness is normalised by the atmospheric pressure (σ_{atm}, 100kPa). A non-dimensional adjustment coefficient ρ of the gradient effect is introduced to represent the possible approximations caused in simplifying the expressions of H_g and l_g in Eq.(7).

3. Rigorous quasi-static cavity expansion analysis

A combination use of small deformation assumption in the elastic zone and large strain analysis for the plastic deformation is adopted (Bigoni and Laudiero, 1989; Chadwick, 1959; Yu and Houlsby, 1991). There are two classes of cavity expansion problems: the general problem of continuous cavity expansion from a finite initial radius and the particular case of the creation of a cavity within an infinite soil mass (Salgado and Randolph, 2001). The total strain method and the incremental velocity approach of similarity solutions are commonly used methods dealing with these two problems (Yu and Carter, 2002). In this paper, the quasi-static expansion analysis is first conducted by using the former method as follows, and a semi-analytical solution based on the second approach is also put forward afterwards.

In the total strain approach, the accumulative geometric changes during strictly symmetric expansions are often described by natural strains (or logarithmic strains) defined in Eq.(8 a,b) without any limitation of the deformation degree.

$$\varepsilon_r = \ln\frac{dr}{dr_0} \quad , \quad \varepsilon_\theta = \ln\frac{r}{r_0} \tag{8 a,b}$$

where ε_r and ε_θ represents the radial strain and tangential strain respectively. r is the current radial distance of a point in the coordinate system as r_0 represents its initial position.

Then, by eliminating r_0, the geometric compatibility condition of large deformations can be derived as

$$[1-e^{(\varepsilon_\theta-\varepsilon_r)}]dr = rd\varepsilon_\theta \tag{9}$$

For small deformation analysis, the compatibility condition is expressed in Eq.(10) following the definitions of $\varepsilon_r = du/dr$ and $\varepsilon_\theta = u/r$ (u represents the radial displacement).

$$\varepsilon_r - \varepsilon_\theta = \frac{rd\varepsilon_\theta}{dr} \tag{10}$$

3.1. Elastic solutions

Initially, the surrounding soil deforms purely elastically. According to the Hooke's law, under conditions of radial symmetry stress-strain relationships in the rate version can be expressed as

$$\dot{\varepsilon}_r^e = \frac{\partial \dot{u}}{\partial r} = \frac{1}{M}[\dot{\sigma}_r - \frac{k\nu}{1-\nu(2-k)}\dot{\sigma}_\theta] \tag{11}$$

$$\dot{\varepsilon}_\theta^e = \frac{\dot{u}}{r} = \frac{1}{M}\left\{-\frac{\nu}{1-\nu(2-k)}\dot{\sigma}_r + [1-\nu(k-1)]\dot{\sigma}_\theta\right\} \tag{12}$$

where $M = \frac{E}{1-\nu^2(2-k)}$. E is Young's modulus. ν is the Poisson's ratio.

Elastic stresses and the radial displacement can be readily derived from the equilibrium equation (Eq.(1)), compatibility equation (Eq.(10)) and stress boundary conditions (Eq.(2 a,b)) as

$$\sigma_r^e = -p_0 - (p - p_0)(\frac{a}{r})^{1+k} \tag{13}$$

$$\sigma_\theta^e = -p_0 + \frac{1}{k}(p - p_0)(\frac{a}{r})^{1+k} \tag{14}$$

$$u^e = r - r_0 = \frac{p - p_0}{2kG}(\frac{a}{r})^{1+k} r \tag{15}$$

3.2. Elastic-plastic analysis

The addition of the second-order strain gradient in the yield criterion applies no influence on directions of the principal stresses in the plastic zone. Hence, the inequalities given in Eq.(16 a,b) are still valid at most cases of the symmetric cavity expansion problem (Gao, 2003a, b; Tsagrakis et al., 2006; Yu and Houlsby, 1991).

$$\sigma_\theta \geq \sigma_z \geq \sigma_r \quad \text{(Cylindrical)} \quad , \quad \sigma_\theta = \sigma_\varphi \geq \sigma_r \quad \text{(Spherical)} \tag{16 a,b}$$

It means that the major and minor principal stress directions stay in the circumferential and radial directions respectively. Hence the modified yield criterion of Eq.(4) can be rewritten as

$$[\alpha + c_g(\frac{k}{r}\frac{\partial\gamma_p}{\partial r} + \frac{\partial^2\gamma_p}{\partial r^2})]\sigma_\theta = \sigma_r \tag{17}$$

Normalising the spatial position of points by the current cavity radius (a) which can be regarded as a 'time scale' during a continuous expansion, the modified friction property becomes

$$\bar{\alpha} = \alpha + \rho\frac{G}{\sigma_{atm}}(\frac{d_{50}}{a})^2(\frac{k}{\bar{r}}\frac{\partial\gamma_p}{\partial\bar{r}} + \frac{\partial^2\gamma_p}{\partial\bar{r}^2}) \tag{18}$$

where $\bar{r} = r/a$. It is clearly shown that both the intrinsic material length (mean particle size) and the instantaneous cavity size are incorporated in the yield function. Under the same strain level, it is shown that the influence of the strain gradient is proportional to the square of d_{50}/a, the value of G/σ_{atm}, and the adjustment coefficient ρ.

As the strain gradient applies no effect when the material just enters the plastic flow state ($\nabla^2\gamma_p\big|_{r=r_c} = 0$), the conventional yield criterion is recovered (i.e., $\alpha\sigma_\theta = \sigma_r$) at the elastic-plastic boundary ($r = r_c$). Based on the radial stress continuity condition, the pressure at the elastic-plastic boundary (p_c) can be obtained by the elastic stress solutions given in Eq.(19). Once the applied internal pressure exceeds the value of p_c, a plastic zone will start forming from the inner cavity wall and continuously enlarge outwards with an increasing expansion pressure.

$$p_c = \frac{k(\alpha-1)p_0}{\alpha+k} + p_0 = 2kG\delta + p_0 \tag{19}$$

where $\delta = \dfrac{(\alpha-1)p_0}{2G(\alpha+k)}$.

According to Eq.(6), plastic components of strain rates can be expressed as

$$\dot{\varepsilon}_{\mathrm{r}}^{\mathrm{p}} = -\dot{\gamma}_{\mathrm{p}} \quad , \quad \dot{\varepsilon}_{\theta}^{\mathrm{p}} = \frac{\beta}{\mathrm{k}}\dot{\gamma}_{\mathrm{p}} \tag{20 a,b}$$

With an associated flow rule (i.e., $\beta = \alpha$), Eqs.(20 a,b) are identical to those derived with the principle of plastic power equivalence by Papanastasiou and Durban (1997). The total strain rates ($\dot{\varepsilon}_{\mathrm{ij}}$) of a given spatial position consist of elastic (i.e., Eqs.(11) and (12)) and plastic components (i.e., Eq.(20 a,b)), that is $\dot{\varepsilon}_{\mathrm{ij}} = \dot{\varepsilon}_{\mathrm{ij}}^{\mathrm{e}} + \dot{\varepsilon}_{\mathrm{ij}}^{\mathrm{p}}$ (Eulerian descriptions). Then integrating them from the initial phase to the current state gives

$$\varepsilon_{\mathrm{r}} = \frac{1}{\mathrm{M}}[\sigma_{\mathrm{r}} - \frac{\mathrm{k}\nu}{1-\nu(2-\mathrm{k})}\sigma_{\theta} + \frac{(1-2\nu)\,\mathrm{p}_0}{1-\nu(2-\mathrm{k})}] - \gamma_{\mathrm{p}} \tag{21}$$

$$\varepsilon_{\theta} = \frac{1}{\mathrm{M}}\left\{ -\frac{\nu}{1-\nu(2-\mathrm{k})}\sigma_{\mathrm{r}} + [1-\nu(\mathrm{k}-1)]\sigma_{\theta} + \frac{(1-2\nu)\,\mathrm{p}_0}{1-\nu(2-\mathrm{k})} \right\} + \frac{\beta}{\mathrm{k}}\gamma_{\mathrm{p}} \tag{22}$$

The conventional boundary conditions are obtained from the stress and strain continuity conditions across the elastic-plastic surface as usual.

$$\sigma_{\mathrm{r}}\big|_{\mathrm{r}=\mathrm{r_c}} = -\mathrm{p_c} \quad , \quad \sigma_{\theta}\big|_{\mathrm{r}=\mathrm{r_c}} = -\mathrm{p}_0 + \frac{1}{\mathrm{k}}(\mathrm{p_c} - \mathrm{p}_0) \quad , \quad \gamma_{\mathrm{p}}\big|_{\mathrm{r}=\mathrm{r_c}} = 0 \tag{23 a,b,c}$$

An extra boundary condition (Eq.(24)) is imposed at the elastic-plastic surface in accordance with the condition that $\delta\gamma_{\mathrm{p}}(\partial\gamma_{\mathrm{p}} / \partial \mathrm{r}) = 0$ (δ denotes the small variation of a quantity) on $\partial\mathrm{V}$ (V denotes the plastic domain) determined from the analysis of an integral formulation of the modified yield function as employed by De Borst and Mühlhaus (1992) and Tsagrakis et al. (2004).

$$\left.\frac{\partial\gamma_{\mathrm{p}}}{\partial\mathrm{r}}\right|_{\mathrm{r}=\mathrm{r_c}} = 0 \tag{24}$$

Substituting Eqs.(21) and (22) into either Eq.(9) for the large strain analysis or Eq.(10) for the small strain analysis, the compatibility equation can be expressed in terms of variables of σ_{r}, σ_{θ} and γ_{p}. Then the governing equation system consisting of the equilibrium equation (i.e., Eqs.(1)), compatibility equation (i.e., Eq.(9) or (10)), and yield function (i.e., Eq.(17)) becomes a typical second-order ordinary differential equation system in terms of three variables of σ_{r}, σ_{θ} and γ_{p}, and it can be calculated numerically following the procedure below with the Cauchy boundary conditions given in Eqs.(2 a,b), (23 a,b,c) and (24).

3.3. Numerical procedure

3.3.1. Continuous cavity expansions from a_0

During initial purely elastic expansions, the entire stress and displacement fields around the cavity can be analytically calculated by the elastic solutions given in Eqs.(13)-(15). Once plastic deformations take place (i.e., $p \geq p_c$), the elastic-plastic expansion response can be modelled by numerically solving the established second-order ordinary differential equation system in Section 3.2. In the numerical computation, all stress and material stiffness terms are normalised by the initial confining pressure (p_0) and the spatial positions are normalised by the current cavity radius (a). Thus the plastic stresses and strains at any expansion stage can be readily computed by integrating the resulting governing equation system in the range of [1, r_c / a] with uses of the given boundary conditions.

In the elastic-plastic analysis of a cavity expanding from a_0 to a, iterations are required to find the one-to-one corresponding relationship between a / a_0 and r_c / a . To improve the computation efficiency, the calculation procedure is subdivided into two phases according to the significantly different responses of soil resistance during continuous expansions. It is found (e.g., in Fig. 2) that r_c / a increases rapidly and monotonically with an increasing internal pressure during initial expansions (phase one) and stabilises soon afterwards with further expansions (phase two). In the phase one, it is easy to model the continuous expansions by assigning increasing values of r_c / a , and corresponding values of a / a_0 can be efficiently obtained by a few steps of iterations. In the phase two, as r_c / a varies in a very small range with increases of a / a_0 and the equation system is highly sensitive to a marginal variation of r_c / a , it is not easy to assign an appropriate initial iteration interval of r_c / a now. Instead it is more tractable to model the subsequent expansions by means of assigning increasing values of a / a_0 and iterate r_c / a . Above integrations are accomplished with the ode113 solver in Matlab (2013a), and iterations are carried out by a bisection iteration technique here. For brevity, the size-dependent solutions are abbreviated as SD solutions in all figures.

3.3.2. Limit expansion pressure of quasi-static cavity expansions

Limit expansion pressure (p_{lim}) during quasi-static expansions is of great interest in practical applications, for example, estimations of the end resistance of cone penetrometers and pile foundations (Randolph et al., 1994; Yu and Mitchell, 1998). The limit pressure is defined here as the required radial pressure at the steady expansion state (i.e., $r_c / a = \text{constant}$) for a cavity expands to a final radius a. p_{lim} can be calculated from a continuous expansion analysis with a sufficiently small value of a_0 (i.e. $(a/a_0) \rightarrow \infty$) or inputting a limit ratio of the radii of the elastic-plastic boundary and cavity wall (i.e. $(r_c/a)_{lim}$) directly in the quasi-static expansion analysis (Yu and Carter, 2002). It was demonstrated in Fig. 2 that the gradient effect on the response of r_c/a to the continuous cavity expansions (or changes of a/a_0) mainly concentrates at the initial expansion stages, and r_c/a of the size dependent solutions will stabilise around the same constant limit value as the corresponding conventional elastic perfectly-plastic solution (e.g., solution of Yu and Houlsby (1991)) at the steady expansion state. According to this feature, it is plausible to suggest that the size-dependent limit pressure can be directly computed by inputting $(r_c/a)_{lim}$ that calculated by the conventional solution into the above calculation procedure. Thus with the known integration range (i.e., [1, $(r_c/a)_{lim}$]), the calculation of p_{lim} can be greatly simplified as no iteration is required any more. In fact, this method is equivalent to regarding the cavity expansion as a similarity process (or expanding from zero radius). Here the analytical solution of Yu and Houlsby (1991) is followed to calculate the value of $(r_c/a)_{lim}$ as presented in the Appendix B.

4. Approximate size-dependent cavity expansion analysis

In the above elastic-plastic analysis based on the flow-version gradient plasticity model, difficulties in finding analytical solutions of the resulting governing equation system mainly stem from the absence of an explicit expression of γ_p in terms of the spatial position. Providing that the elastic strain increments are negligible compared to the plastic strain increments (namely, $\dot{\varepsilon}_{ij}^e = 0$ in the plastic zone), γ_p can be obtained prior to knowing the plastic stress field. This simplifying assumption can be expressed as

$$\dot{\varepsilon}_r = \dot{\varepsilon}_r^p = -\dot{\gamma}_p \quad , \quad \dot{\varepsilon}_\theta = \dot{\varepsilon}_\theta^p = \frac{\beta}{k}\dot{\gamma}_p \tag{25 a,b}$$

Integrating Eq.(25 a,b) from r_c to r gives

$$\varepsilon_r = -\gamma_p + \varepsilon_r^e\big|_{r=r_c} \quad , \quad \varepsilon_\theta = \frac{\beta}{k}\gamma_p + \varepsilon_\theta^e\big|_{r=r_c} \tag{26 a,b}$$

Then explicit expressions of γ_p are available as follows based on the compatibility condition.

4.1. Approximate analytical finite strain solutions

Recalling the compatibility condition with finite strain definitions (i.e., Eq.(9)), a simple differential equation of γ_{p} is built as

$$\frac{\mathrm{k}}{\beta}\frac{\mathrm{dr}}{\mathrm{r}}=\frac{\mathrm{d}\gamma_{\mathrm{p}}}{1-\mathrm{e}^{[(\beta/\mathrm{k}+1)\gamma_{\mathrm{p}}+(\mathrm{k}+1)\delta]}} \tag{27}$$

With the boundary condition of Eq.(23 c), γ_{p} in terms of the spatial position goes to

$$\gamma_{\mathrm{p}}=\frac{\mathrm{k}}{\beta+\mathrm{k}}\left\{\ln[\frac{\mathrm{r}^{(\mathrm{k}/\beta+1)}}{\mathrm{C}_1+\mathrm{r}^{(\mathrm{k}/\beta+1)}}]-(\mathrm{k}+1)\delta\right\} \tag{28}$$

where the integration constant $\mathrm{C}_1=\eta \mathrm{r}_{\mathrm{c}}^{(\frac{\mathrm{k}}{\beta}+1)}$ with $\eta=\mathrm{e}^{-(\mathrm{k}+1)\delta}-1$.

Then the Laplacian of γ_{p} leads to

$$\nabla^2\gamma_{\mathrm{p-c}}=-(\frac{\beta+1}{\beta^2})\frac{\mathrm{C}_1\mathrm{r}^{(1/\beta-1)}}{[\mathrm{C}_1+\mathrm{r}^{(1/\beta+1)}]^2} \qquad \text{(Cylindrical)} \tag{29}$$

$$\nabla^2\gamma_{\mathrm{p-s}}=\frac{2\mathrm{C}_1}{\beta^2}\frac{[\beta\mathrm{C}_1-2\mathrm{r}^{(2/\beta+1)}]}{\mathrm{r}^2[\mathrm{C}_1+\mathrm{r}^{(2/\beta+1)}]^2} \qquad \text{(Spherical)} \tag{30}$$

Now the defined problem becomes to find the solution of Eq.(31) with the conventional boundary conditions of Eqs. (2 a,b) and (23 a,b,c).

$$\frac{\mathrm{d}\sigma_{\mathrm{r}}}{\sigma_{\mathrm{r}}}=\frac{\mathrm{k}}{\mathrm{r}}(\frac{1}{\bar{\alpha}}-1)\mathrm{dr} \tag{31}$$

As a result, the internal expansion pressure is equal to

$$\mathrm{p}=\mathrm{p}_{\mathrm{c}}(\frac{\mathrm{r}_{\mathrm{c}}}{\mathrm{r}})^{\mathrm{k}(1-\frac{1}{\alpha})}\exp[-\int_{\mathrm{a}}^{\mathrm{r}_{\mathrm{c}}}\frac{\mathrm{k}}{\mathrm{r}}(\frac{1}{\bar{\alpha}}-\frac{1}{\alpha})\mathrm{dr}] \tag{32}$$

The propagation of the elastic-plastic boundary during continuous expansions can be described by substituting the logarithm strains into the compressibility equation of Eq.(33).

$$\beta\varepsilon_{\mathrm{r}}+\mathrm{k}\varepsilon_{\theta}=\beta\,\varepsilon_{\mathrm{r}}^{\mathrm{e}}\Big|_{\mathrm{r}=\mathrm{r}_{\mathrm{c}}}+\mathrm{k}\varepsilon_{\theta}^{\mathrm{e}}\Big|_{\mathrm{r}=\mathrm{r}_{\mathrm{c}}}=(1-\beta)\mathrm{k}\delta \tag{33}$$

with a solution of

$$\frac{\mathrm{r}_{\mathrm{c}}}{\mathrm{a}}=[\frac{1-\mathrm{e}^{(1-\beta)\mathrm{k}\delta/\beta}(\mathrm{a}_0/\mathrm{a})^{(\mathrm{k}/\beta+1)}}{1-\mathrm{e}^{(1-\beta)\mathrm{k}\delta/\beta}(1-\delta)^{(\mathrm{k}/\beta+1)}}]^{\frac{\beta}{\beta+\mathrm{k}}} \tag{34}$$

The quasi-static pressure-expansion response now can be approximately modelled with the use of Eqs. (32) and (34).

4.2. Approximate analytical small strain solutions

For a cavity with infinitesimal expansions, the compatibility condition of Eq.(10) is often used to describe the geometric variations for simplicity. The equivalent plastic shear strain and corresponding Laplacian expressions can be obtained following the same procedure as above.

$$\gamma_p^s = \frac{k(k+1)\delta}{k+\beta}[(\frac{r_c}{r})^{(\frac{k}{\beta}+1)} - 1] \tag{35}$$

$$\nabla^2 \gamma_p^s = (k+1)\delta[\frac{\beta(2-k)+k^2}{\beta^2}]\frac{r_c^{(k/\beta+1)}}{r^{(k/\beta+3)}} \tag{36}$$

where the superscript of γ_p^s indicates the small strain definition.

Substituting Eq.(36) into Eq.(31), an analytical stress solution can be derived with the given conventional stress boundary conditions as

$$\sigma_r = -p_c(\frac{r_c}{r})^{k(1-\frac{1}{\alpha})}\left[\frac{(k+1)\delta}{\alpha}[\frac{\beta(2-k)+k^2}{\beta^2}](\frac{r_c}{r})^{(\frac{k}{\beta}+1)}\frac{c_g}{r^2}+1\right]^{\frac{k}{\alpha}\frac{\beta}{(k+3\beta)}} \tag{37}$$

And the radial displacement (u_p^s) in the plastic zone is equal to

$$u_p^s = r - r_0 = r\delta\left\{\frac{(k+1)\beta}{\beta+k}[(\frac{r_c}{r})^{(1+\frac{k}{\beta})} - 1] + 1\right\} \tag{38}$$

The strain gradient effect to the quasi-static cavity expansion response can be more straightforwardly identified in above analytical solutions. The analytical solutions may be useful in benchmark exercises for the validation of numerical codes. Comparing to the corresponding elastic perfectly-plastic solutions (e.g., Bigoni and Laudiero (1989); Yu and Houlsby (1991)), additional terms due to the gradient effect are included in the stress solutions of both Eqs.(32) and (37). As a result, the stresses now are not only dependent on the non-dimensional quantity of r_c / r as usual but also on the square of d_{50} / r. Thus the particle size effect and cavity size effect are theoretically captured. While the gradient effect vanishes (c_g =0, or $(d_{50} / r)^2 \propto 0$), the conventional stress solution can be recovered exactly. In addition, due to the ignorance of the elastic strain increments in the plastic region, no gradient effect appears in the displacement solutions of the simplified cases. Setting the left part of Eq.(33) as zero, Eq.(34) is the same as the conventional solution that derived by ignoring all the elastic strain in the plastic region.

5. Results and discussion

A selection of results is now presented to highlight and discuss the size-dependent cavity expansion response due to the inclusion of the strain gradient in the yield criterion. Typical values of $p_0 = 50\text{kPa}$, $G / p_0 = 350$, $\nu = 0.3$ are set unless redefinitions in the following calculations.

5.1. Strain gradient effect on stress and strain distributions

It is shown (e.g., Eq.(18)) that the introduced strain gradient (Laplacian) consists of the first and second order space derivatives with respect to γ_p. Therefore, at a given expansion instant, the gradient effect depends on the spatial variation of γ_p. Taking results in Fig. 3 as an example, it is shown that, as other strain components, γ_p decreases rapidly along the radial direction, especially in a close vicinity of the inner cavity, and then slowly converges to zero outwards from this localised zone. This strain concentration phenomenon intensifies with an increasing expansion level and is more significant during expansions of a spherical cavity. As a consequence, the gradient effect may gradually attenuate with an increasing distance away from the inner cavity wall and vanish soon outside of the inner annulus within which dramatic strain variations occur. For example, Fig. 4 shows that the size-dependent solutions predict greater radial compression stresses and lower circumferential stresses around the inner cavity than the conventional elastic perfectly-plastic solution of Yu and Houlsby (1991), and the differences gradually disappear while moving outwards. Meanwhile, Fig. 4 (a) and (b) demonstrate that solutions based on the large strain and small strain compatibility conditions naturally give almost the same results at small degrees of the cavity expansion. It should be borne in mind that, as no tensile strength was applied in the present strain gradient plasticity model of sand, both the radial and circumferential stresses stay under compression in the plastic domain. In addition, as pointed out by De Borst and Mühlhaus (1992), the introduction of higher-order spatial gradients corresponds to a singular perturbation of the original yield criterion. The second-order gradient may bring short-wavelength terms into the governing equations during numerical computations, which leads to periodic variations (or oscillation) of the circumferential stress in the plastic domain (Holmes, 2012), especially at initial expansion stages with a relatively thin plastic region (e.g. Fig. 4). As the circumferential stress may infinitely approach zero around the cavity wall due to the gradient effect, caution should be taken in the numerical calculation.

Comparing between the size-dependent solution and the conventional solution, although the plastic stress field is significantly altered around the localised deformation zone, Fig. 3 shows that marginal changes of the strain distribution are produced mainly due to the same plastic flow rule is adopted. Meanwhile, as discussed above, the gradient effect to the plastic stresses concentrates in a very thin region and rapidly vanishes far before reaching the elastic-plastic boundary. These characteristics lead to that the relative propagation of the plastic zone during expansions (i.e., r_c / a) calculated with and without considering the gradient effect are almost the same, especially at relatively large cavity radii, as shown in Fig. 2.

5.2. Size-dependent continuous pressure-expansion response

The size-dependent pressure-expansion response during quasi-static cavity expansions is analysed first by using the method outlined in Section 3.3.1. During continuous expansions of a cavity from a_0 to a , a / a_0 reflects the cumulative deformation level; r_c / a indicates the state of the pressure-expansion response (or relative propagation speed of the plastic region). In addition to these two normalised size parameters, Eq.(18) displayed that d_{50} / a also plays a role in determining the overall plastic soil response to cavity expansions in the present model. Among them, d_{50} and a_0 are necessary initial information for the continuous expansion analysis now. d_{50} is easy to be obtained from the particle size distribution curve. a_0 is roughly estimated by values in a range around $d_{50}/5$ in the following calculations for illustration.

Fig. 5 shows that, comparing with the conventional elastic perfectly-plastic solution of Yu and Houlsby (1991), a stiffer initial elastic-plastic response is predicted by the size-dependent solution, for example, higher peak values of the internal expansion pressure. The peak radial pressure is reached around the same deformation/expansion level before entering the steady deformation state (i.e., r_c / a plateaued), but it is higher for a cavity expanding from a smaller initial radius since the greater corresponding value of d_{50} / a at peaks. With the same value of d_{50} in a given sand, the required expansion pressure depends not only on the non-dimensional geometric size of r_c / a or a / a_0 but also on the real cavity size independently in the size-dependent solution. After the peak, the internal radial pressure gradually decreases with further expansions and converges to the conventional solution after a sufficiently large expansion. It implies that the strain gradient effect vanishes and the conventional plasticity model is recovered eventually with a sufficiently small value of d_{50} / a . In addition, the influence of the introduced adjustment coefficient ρ is illustrated in Fig. 6. Before the strain gradient becomes ineffective, larger radial expansion pressures are predicted by the size-dependent solution with greater values of ρ due to the greater contribution of the strain gradient to the local soil strength.

Overall, in contrast to the conventional elastic perfectly-plastic solution in which the required expansion pressure is solely dependent on the non-dimensional values of r_c / a or a/a_0 with given soil properties and boundary conditions, it is demonstrated that the size-dependent solution predicts that the geometric sizes of a_0, a, and d_{50} all exert their own influences on the continuous pressure-expansion response, which may theoretically account for the aforementioned size-strengthening phenomenon associated with the particle size effect and the cavity size effect.

5.3. Size-dependent limit expansion pressure

It was suggested in Section 3.3.2 that the limit pressure p_{lim} of a cavity expanding to a given final radius can be calculated either from the continuous expansion analysis with a sufficiently small value of a_0 (approximately, $a_0 < a / 20$) or by directly using the constant value of $(r_c / a)_{lim}$ at the steady expansion state in the integration. Results computed by these two methods are compared in Fig. 7 and Fig. 8, and excellent consistencies are shown in all cases of various levels of the strain gradient effect as expected. It is demonstrated that the simplified method can provide an efficient and accurate alternative to calculate p_{lim}. Comparing with the counterpart conventional solution, due to the marginal influence of the introduced strain gradient to $(r_c / a)_{lim}$, constant limit expansion pressures is approached at similar accumulative expansion levels in the size-dependent solution. The size-dependent p_{lim} equals the maximum expansion pressure required for a cavity expands to a final radius of a. Using the simplified method, the size-dependent behaviour of p_{lim} is more clearly presented in Fig. 9 and Fig. 10 with a range of typical strength and stiffness parameters of sand. It is shown that the limit expansion pressure gets higher with larger values of d_{50} / a and/or ρ in the size-dependent solutions. However, no such size-dependent variations can be predicted by the conventional cavity expansion solution.

Based on the analogy between quasi-static cavity expansion and cone penetration, the limit expansion pressure is widely applied to estimate the cone resistance in CPTs (Yu, 2000, 2006). As previously mentioned, it is often observed that higher resistances are experienced by smaller penetrometers in both laboratory tests and site investigations (Balachowski, 2007; Bolton et al., 1999; De Beer, 1963; Eid, 1987; Junior et al., 2014; Lima and Tumay, 1991; Sudduth et al., 2004; Whiteley and Dexter, 1981; Wu and Ladjal, 2014). For example, statistical analysis of a number of in-situ cone penetration tests showed that the cone tip resistance measured by a 12.7mm sized cone penetrometer is 18% higher than that measured by the standard penetrometer (35.7mm in diameter), and no significant variation was found between the standard and 43.7mm sized cone penetrometer (Lima and Tumay, 1991); 10% higher in average of the tip resistance is measured by a 16.0mm sized penetrometer than the standard cone penetrometer (Kurup and Tumay, 1998; Tumay et al., 2001). In CPTs performed with the "modelling of models" method in sand on the centrifuge platform, it is generally observed that the particle size effect may gradually enhance with decreases of D_{CPT} / d_{50} (D_{CPT} represent the cone diameter), especially while D_{CPT} / d_{50} is less than 20 (Balachowski, 2007; Bolton et al., 1999; Sharp et al., 2010). These experimental findings are consistent with the size effect predicted by the size-dependent solution in trend (e.g., Fig. 9). According to the close relevance between the limit expansion pressure and the cone resistance (Yu and Mitchell, 1998), the size-dependent solution may provide a possible theoretical method to account for the size effects in CPTs. Or reversely, cone penetrometers of different sizes may provide an effective physical means to explore the soil properties in different size scales, for example, to investigate the strain gradient dependency of soil strength introduced in the present model (e.g., c_g).

5.4. Size-dependent solutions of special cases

The radial pressure-expansion curve at initial expansion stages is also of practical use in the interpretation of in situ testing with small deformations, for example, self-boring pressuremeter tests (Ahmadi and Keshmiri, 2017; Hughes et al., 1977). The size-dependent pressure-expansion responses at initial expansion stages calculated by different methods are presented in Fig. 11. It is shown that the small strain solution and the large strain solution give close results at small deformations (normally, $a / a_0 \leq 1.2$). With increasing deformation levels, the small strain solution tends to over-predict the required internal expansion pressure.

Bigoni and Laudiero (1989) pointed out that neglecting all elastic deformations in the plastic region may lead to significant overestimations of the internal pressure in both cylindrical and spherical cavity expansion solutions based on the conventional Mohr-Coulomb criterion. Although parts of the elastic strains in the plastic region have been considered in the present approximate solutions, evident over-predictions still are produced with comparisons to the rigorous solutions both at small deformations and during large expansions as shown in Fig. 11 and Fig. 12 respectively. The over-prediction gets more severe when the strain gradient effect is included, especially during the expansion analysis of a spherical cavity. These result comparisons indicate that the elastic components of total strains in the plastic domain play an important role in the quasi-static cavity pressure-expansion response.

6. Conclusions

Based on a modified Mohr-Coulomb yield criterion incorporating the strain gradient effect, unified size-dependent finite strain solutions are presented for the quasi-static expansion analysis of both cylindrical and spherical cavities in an infinite medium. A simple numerical method was developed for modelling the continuous cavity expansion, and a simplified method without iterations was proposed for calculating the size-dependent limit pressure.

Due to the inclusion of a second-order strain gradient into the yield stress, two new material parameters, an intrinsic material length (l_g) and a non-dimensional modulus index regulating the gradient effect (H_g), and one extra boundary condition were introduced in the strain gradient model. The new material parameters were expressed in terms of the conventional parameters of sand (i.e., d_{50} and G/σ_{atm}) with an additional adjustment coefficient ρ. In the quasi-static cavity expansion problem, it is shown that the introduced strain gradient effect depends on the accumulation and distribution of the plastic strain and is proportional to the square of d_{50}/a and ρ. As a result, the size-strengthening effects associated with the particle size and the instantaneous cavity size are captured by the new solutions. By comparing with the counterpart conventional solutions, stiffer soil responses are generally predicted by the strain gradient plasticity model in a vicinity of the inner cavity, for example, higher radial stresses, but it was found that the gradient effect applies slight influences on the propagation of the plastic zone and r_c/a will eventually stabilize around almost the same constant limit value at the steady expansion state. The gradient effect will vanish with sufficient small values of d_{50}/a and/or ρ, and the conventional elastic perfectly-plastic solutions can be exactly recovered then. The size-dependent solutions may provide a theoretical method to account for the structure size effect and sand particle size effect that often observed in some small-scale sand-structure interaction problems.

In addition, by neglecting the elastic increments of strains in the plastic region, approximate analytical size-dependent solutions were also derived. The gradient effect to the quasi-static problem is more explicitly expressed in the analytical solutions. However, it was shown that the elastic strains in the plastic zone play an important role in the continuous cavity expansion analysis, and significant overpredictions could be produced if they are neglected.

Appendix A

It is assumed that the stresses at one point x are determined by deformation histories of all points in the volume V of a RVE (Mühlhaus and Aifantis, 1991; Vardoulakis and Aifantis, 1991). V reflects a phenomenal scope of nonlocal contributing points with a radius of R_g ($V = 4\pi R_g^{\ 3}/3$ in three dimensions and $V = \pi R_g^{\ 2}$ for the plane problem). Thus the average strain $\bar{\gamma}_p$ within a symmetric neighbourhood of x can be expressed by the Taylor series expansion as

$$\bar{\gamma}_p = \frac{1}{V}\int_V \dot{\gamma}_p(x_i + \xi_i) d_V \tag{A- 1}$$

$$\dot{\gamma}_p(x_i + \xi_i) = \dot{\gamma}_p(x_i) + \nabla\dot{\gamma}_p(x_i)\xi_j + \frac{1}{2!}\nabla^2\dot{\gamma}_p(x_i)\xi_j\xi_k + \cdots \tag{A- 2}$$

where ξ_i is a vector along the radial direction and $|\xi_i| \le R_g$. ∇ is the gradient operator, and $\nabla^2\cdot = \nabla(\nabla\cdot)$. Substituting Eq.(A- 2) into Eq.(A- 1) gives

$$\bar{\gamma}_p = \gamma_p(x_i) + \frac{1}{\pi R_g^{\ 2}}\left[\frac{R_g^{\ 3}}{3}\nabla\gamma_p(x_i)\int_0^{2\pi} n_j d_\theta + \frac{1}{2!}\frac{R_g^{\ 3}}{4}\nabla^2\gamma_p(x_i)\int_0^{2\pi} n_j n_k d_\theta + \cdots\right] \quad \text{(2 dimensional)} \tag{A- 3}$$

where $\int_0^{2\pi} n_j d_\theta = 0$, $\int_0^{2\pi} n_j n_k d_\theta = \pi\delta_{ij}$ (i from 1 to 2).

$$\bar{\gamma}_p = \gamma_p(x_i) + \frac{3}{4\pi R_g^{\ 3}}\left[\frac{R_g^{\ 4}}{3}\nabla\gamma_p(x_i)\int_0^{2\pi} n_j d_\theta + \frac{1}{2!}\frac{4R_g^{\ 5}}{15}\nabla^2\gamma_p(x_i)\int_0^{2\pi} n_j n_k d_\theta + \cdots\right] \quad \text{(3 dimensional)} \tag{A- 4}$$

where $\int_0^{2\pi} n_j d_\theta = 0$, $\int_0^{2\pi} n_j n_k d_\theta = \frac{2\pi}{3}\delta_{ij}$ (i from 1 to 3).

Appendix B

The solution of Yu and Houlsby (1991) (i.e., Eqs.(B-1) and (B-2)) is followed to calculate $(r_c / a)_{lim}$.

$$(r_c / a)_{lim} = R_\infty^{\ \alpha/[k(\alpha-1)]} \tag{B-1}$$

$$\Lambda_1(R_\infty, \xi_1) = (\eta_1 / \gamma_1)(1-\delta)^{(\beta+k)/\beta} \tag{B-2}$$

where $\Lambda_1(x, y)=\sum_{n=0}^{\infty} A_n^1$

$$A_n^1=\begin{cases} \dfrac{y^n}{n!}\ln x & ,\text{if} \quad n-\gamma_1 \\ \dfrac{y^n}{n!(n-\gamma_1)}[x^{(n-\gamma_1)}-1] & ,\text{otherwise} \end{cases}$$

$$\gamma_1=\frac{\alpha(\beta+k)}{k(\alpha-1)\beta}$$

$$\eta_1=\exp\left\{\frac{(\beta+k)(1-2\nu)(\alpha-1)\,p_0[1+\nu(2-k)]}{E(\alpha-1)\beta}\right\}$$

$$\xi_1=\frac{[1-\nu^2(2-k)](1+k)\delta}{(1+\nu)(\alpha-1)\beta}\left[\alpha\beta+k(1-2\nu)+2\nu-\frac{k\nu(\alpha+\beta)}{1-\nu(2-k)}\right].$$

Acknowledgements

The present work was partly conducted at the Nottingham Centre for Geomechanics (NCG). The first author would like to acknowledge the financial support provided by the University of Nottingham and the China Scholarship Council for his PhD study.

References

Ahmadi, M.M., Keshmiri, E., 2017. Interpretation of in situ horizontal stress from self-boring pressuremeter tests in sands via cavity pressure less than limit pressure: a numerical study. Environmental Earth Sciences. 9 (76), 1-17.

Aifantis, E.C., 1987. The physics of plastic deformation. International Journal of Plasticity. 3 (3), 211-247.

Aifantis, E.C., 1996. Higher order gradients and size effects, in: Carpinteri, A. (Ed.), Size-scale effects in the failure mechanisms of materials and structures, E & FN Spon, London, pp. 231-242.

Aifantis, E.C., 1999. Strain gradient interpretation of size effects. International Journal of Fracture. 95 (1), 299-314.

Aifantis, E.C., 2003. Update on a class of gradient theories. Mechanics of Materials. 35 (3), 259-280.

Al Hattamleh, O., Muhunthan, B., Zbib, H.M., 2004. Gradient plasticity modelling of strain localization in granular materials. International Journal for Numerical and Analytical Methods in Geomechanics. 28 (6), 465-481.

Athani, S., Kharel, P., Airey, D., Rognon, P., 2017. Grain-size effect on uplift capacity of plate anchors in coarse granular soils. Géotechnique Letters. 7 (2), 167-173.

Balachowski, L., 2006. Scale effect in shaft friction from the direct shear interface tests. Archives of Civil and Mechanical Engineering. 6 (3), 13-28.

Balachowski, L., 2007. Size effect in centrifuge cone penetration tests. Archives of Hydro-Engineering and Environmental Mechanics. 54 (3), 161-181.

Bigoni, D., Laudiero, F., 1989. The quasi-static finite cavity expansion in a non-standard elasto-plastic medium. International Journal of Mechanical Sciences. 31 (11), 825-837.

Bishop, R.F., Hill, R., Mott, N.F., 1945. The theory of indentation and hardness tests. The proceedings of the Physical Society. 57 (3), 147–159.

Bolton, M.D., 1986. The strength and dilatancy of sands. Geotechnique. 36 (1), 65-78.

Bolton, M.D., Gui, M.W., Garnier, J., Corte, J.F., Bagge, G., Laue, J., Renzi, R., 1999. Centrifuge cone penetration tests in sand. Geotechnique. 49, 543-552.

Chadwick, P., 1959. The quasi-static expansion of a spherical cavity in metals and ideal soils. The Quarterly Journal of Mechanics and Applied Mathematics. 12 (1), 52-71.

Chakraborty, T., Salgado, R., 2010. Dilatancy and shear strength of sand at low confining pressures. Journal of Geotechnical and Geoenvironmental Engineering. 136 (3), 527-532.

Chow, F.C., 1996. Investigations into the behaviour of displacement piles for offshore foundations (Ph.D. thesis). University of London (Imperial College), U.K.

Collin, F., Caillerie, D., Chambon, R., 2009. Analytical solutions for the thick-walled cylinder problem modeled with an isotropic elastic second gradient constitutive equation. International Journal of Solids and Structures. 46 (22), 3927-3937.

Collins, I.F., Yu, H.S., 1996. Undrained cavity expansions in critical state soils. International Journal for Numerical and Analytical Methods in Geomechanics. 20 (7), 489-516.

De Beer, E.E., 1963. The scale effect in the transposition of the results of deep-sounding tests on the ultimate bearing capacity of piles and caisson foundations. Geotechnique. 13 (1), 39-75.

De Borst, R., Mühlhaus, H.B., 1992. Gradient‐dependent plasticity: Formulation and algorithmic aspects. International Journal for Numerical Methods in Engineering. 35 (3), 521-539.

Eid, W.K., 1987. Scaling effect in cone penetration testing in sand (Ph.D. thesis). Virginia Polytechnic Institute, Blacksburg, VA. USA.

Eshel, N.N., Rosenfeld, G., 1970. Effects of strain-gradient on the stress-concentration at a cylindrical hole in a field of uniaxial tension. Journal of Engineering Mathematics. 4 (2), 97-111.

Fleck, N., Hutchinson, J., 1997. Strain gradient plasticity. Advances in Applied Mechanics. 33, 295-361.

Gao, H., Huang, Y., Nix, W., Hutchinson, J., 1999. Mechanism-based strain gradient plasticity-I. Theory. Journal of the Mechanics and Physics of Solids. 47 (6), 1239-1263.

Gao, X.L., 2002. Analytical solution of a borehole problem using strain gradient plasticity. Journal of Engineering Materials and Technology. 124 (3), 365-370.

Gao, X.L., 2003a. Elasto-plastic analysis of an internally pressurized thick-walled cylinder using a strain gradient plasticity theory. International Journal of Solids and Structures. 40 (23), 6445-6455.

Gao, X.L., 2003b. Strain gradient plasticity solution for an internally pressurized thick-walled spherical shell of an elastic–plastic material. Mechanics Research Communications. 30 (5), 411-420.

Gao, X.L., 2006. An expanding cavity model incorporating strain-hardening and indentation size effects. International Journal of Solids and Structures. 43 (21), 6615-6629.

Gibson, R.E., Anderson, W.F., 1961. In situ measurement of soil properties with the pressuremeter. Civil Engineering and Public Works Review. 56 (658), 615-618.

Gudmundson, P., 2004. A unified treatment of strain gradient plasticity. Journal of the Mechanics and Physics of Solids. 52 (6), 1379-1406.

Guo, P., Stolle, D., 2005. Lateral Pipe-Soil Interaction in Sand with Reference to Scale Effect. Journal of Geotechnical and Geoenvironmental Engineering. 131 (3), 338-349.

Hill, R., 1950. The mathematical theory of plasticity. Oxford University Press, London.

Holmes, M.H., 2012. Introduction to perturbation methods. Springer Science & Business Media, New York.

Huang, Y., Qu, S., Hwang, K., Li, M., Gao, H., 2004. A conventional theory of mechanism-based strain gradient plasticity. International Journal of Plasticity. 20 (4), 753-782.

Hughes, J.M.O., Wroth, C.P., Windle, D., 1977. Pressuremeter tests in sands. Geotechnique. 27 (4), 455-477.

Hutchinson, J.W., 2012. Generalizing J2 flow theory: Fundamental issues in strain gradient plasticity. Acta Mechanica Sinica. 28 (4), 1078-1086.

Junior, D.D.V., Biachini, A., Valadão, F.C.A., Rosa, R.P., 2014. Penetration resistance according to penetration rate, cone base size and different soil conditions. Bragantia. 73 (2), 171-177.

Kurup, P.U., Tumay, M.T., 1998. Calibration of a miniature cone penetrometer for highway applications. Transportation Research Record: Journal of the Transportation Research Board. 1614 (1), 8-14.

Ladjal, S., 2013. Scale effect of cavity expansion in soil with application to plant root growth (P.h.D thesis). University of Natural Resources and Life Sciences, Vienna, Austria.

Lehane, B.M., Gaudin, C., Schneider, J.A., 2005. Scale effects on tension capacity for rough piles buried in dense sand. Geotechnique. 55 (10), 709-719.

Lima, D.C.d., Tumay, M.T., 1991. Scale effects in cone penetration tests, Geotechnical Engineering Congress—1991. ASCE, pp. 38-51.

Meyerhof, G.G., 1983. Scale effects of ultimate pile capacity. Journal of Geotechnical Engineering. 109 (6), 797-806.

Mindlin, R.D., 1964. Micro-structure in linear elasticity. Archive for Rational Mechanics and Analysis. 16 (1), 51-78.

Mitchell, J.K., Soga, K., 2005. Fundamentals of soil behavior (3rd edn.). John Wiley & Sons, Inc.

Mo, P.Q., Yu, H.S., 2016. Undrained cavity expansion analysis with a unified state parameter model for clay and sand. Geotechnique. 1-13.

Mühlhaus, H.-B., Aifantis, E.C., 1991. A variational principle for gradient plasticity. International Journal of Solids and Structures. 28 (7), 845-857.

Papanastasiou, P., Durban, D., 1997. Elastoplastic analysis of cylindrical cavity problems in geomaterials. International Journal for Numerical and Analytical Methods in Geomechanics. 21 (2), 133-149.

Randolph, M.F., Dolwin, R., Beck, R., 1994. Design of driven piles in sand. Geotechnique. 44 (3), 427-448.

Russell, A.R., Khalili, N., 2006. On the problem of cavity expansion in unsaturated soils. Computational Mechanics. 37 (4), 311-330.

Sakai, T., Erizal, V., Tanaka, T., 1998. Particle size effect of anchor problem with granular materials, Application of Numerical Methods to Geotechnical Problems. Springer, pp. 191-200.

Salgado, R., Mitchell, J.K., Jamiolkowski, M., 1997. Cavity expansion and penetration resistance in sand. Journal of Geotechnical and Geoenvironmental Engineering. 123 (4), 344-354.

Salgado, R., Randolph, M.F., 2001. Analysis of cavity expansion in sand. International Journal of Geomechanics. 1 (2), 175-192.

Schanz, T., Vermeer, P.A., 1996. Angles of friction and dilatancy of sand. Geotechnique. 46 (1), 145-151.

Sharp, M.K., Dobry, R., Phillips, R., 2010. CPT-based evaluation of liquefaction and lateral spreading in centrifuge. Journal of Geotechnical and Geoenvironmental Engineering. 136 (10), 1334-1346.

Sudduth, K.A., Hummel, J.W., Drummond, S.T., 2004. Comparison of the Veris Profiler 3000 to an ASAE-standard penetrometer. Applied Engineering in Agriculture. 20 (5), 535-541.

Tagaya, K., F.Scott, R., Aboshi, H., 1988. Scale effect in anchor pullout test by centrifugal technique. Soils and Foundations. 28 (3), 1-12.

Toupin, R.A., 1962. Elastic materials with couple-stresses. Archive for Rational Mechanics and Analysis. 11 (1), 385-414.

Tsagrakis, I., Efremidis, G., Aifantis, E.C., 2004. Size effects in thick-walled hollow cylinders: deformation versus flow theory of gradient plasticity. Journal of the Mechanical Behavior of Materials. 15 (3), 149-168.

Tsagrakis, I., Efremidis, G., Konstantinidis, A., Aifantis, E.C., 2006. Deformation vs. flow and wavelet-based models of gradient plasticity: Examples of axial symmetry. International Journal of Plasticity. 22 (8), 1456-1485.

Tumay, M.T., Titi, H.H., Senneset, K., Sandven, R., 2001. Continuous intrusion miniature piezocone penetration test in quick soil deposits, Proceedings of the Fifteenth International Conference on Soil Mechanics and Geotechnical Engineering, Istanbul, Turkey, 27-31 August 2001. Volumes 1-3. AA Balkema, pp. 523-526.

Turner, J.P., Kulhawy, F.H., 1994. Physical modeling of drilled shaft side resistance in sand. Geotechnical Testing Journal. 17 (3), 282-290.

Vardoulakis, I., Aifantis, E.C., 1989. Gradient dependent dilatancy and its implications in shear banding and liquefaction. Ingenieur-Archiv. 59 (3), 197-208.

Vardoulakis, I., Aifantis, E.C., 1991. A gradient flow theory of plasticity for granular materials. Acta Mechanica. 87 (3-4), 197-217.

Wernick, E., 1978. Skin friction of cylindrical anchors in non-cohesive soils, Symposium on Soil Reinforcing and Stabilising Techniques, Sydney, pp. 201-219.

Whiteley, G.M., Dexter, A.R., 1981. The dependence of soil penetrometer pressure on penetrometer size. Journal of Agricultural Engineering Research. 26 (6), 467-476.

Wu, W., Ladjal, S., 2014. Scale effect of cone penetration in sand, 3rd International Symposium on Cone Penetration Testing, Las Vegas, Nevada, USA, pp. 459-465.

Yu, H.S., 2000. Cavity expansion methods in geomechanics. Kluwer Academic Publishers, The Netherlands.

Yu, H.S., 2006. The First James K. Mitchell Lecture In situ soil testing: from mechanics to interpretation. Geomechanics and Geoengineering: An International Journal. 1 (3), 165-195.

Yu, H.S., Carter, J.P., 2002. Rigorous similarity solutions for cavity expansion in cohesive-frictional soils. International Journal of Geomechanics. 2 (2), 233-258.

Yu, H.S., Houlsby, G.T., 1991. Finite cavity expansion in dilatant soils: loading analysis. Geotechnique. 41 (2), 173-183.

Yu, H.S., Mitchell, J.K., 1998. Analysis of cone resistance: review of methods. Journal of Geotechnical and Geoenvironmental Engineering. 124 (2), 140-149.

Zbib, H.M., 1994. Strain gradients and size effects in nonhomogeneous plastic deformation. Scripta Metallurgica et Materialia. 30 (9), 1223-1226.

Zbib, H.M., Aifantis, E.C., 1989. A gradient-dependent flow theory of plasticity: application to metal and soil instabilities. Applied Mechanics Reviews. 42 (11), S295-S304.

Zervos, A., Papanastasiou, P., Vardoulakis, I., 2001. A finite element displacement formulation for gradient elastoplasticity. International Journal for Numerical Methods in Engineering. 50, 1369-1388.

Zhao, J., 2011. A unified theory for cavity expansion in cohesive-frictional micromorphic media. International Journal of Solids and Structures. 48 (9), 1370-1381.

Zhao, J., Sheng, D., Sloan, S.W., Krabbenhoft, K., 2007. Limit theorems for gradient-dependent elastoplastic geomaterials. International Journal of Solids and Structures. 44 (2), 480-506.

Zhao, J., Sheng, D., Zhou, W., 2005. Shear banding analysis of geomaterials by strain gradient enhanced damage model. International Journal of Solids and Structures. 42 (20), 5335-5355.

Zhou, W., Zhao, J., Liu, Y., Yang, Q., 2002. Simulation of localization failure with strain-gradient-enhanced damage mechanics. International journal for numerical and analytical methods in geomechanics. 26 (8), 793-813.

MATLAB 2013a, The MathWorks, Inc., Natick, Massachusetts, United States.

Figures

Fig. 1 Example boundary conditions during expansions of a cylindrical cavity

Fig. 2 Propagation of elastic-plastic boundaries during expansions ($p_0 = 50\text{kPa}$, $G / p_0 = 350$, $\varphi = 40^o$, $\psi = 15^o$, $\nu = 0.3$, $d_{50} = 1\text{mm}$)

Fig. 3 Strain distributions at different expansion instants

Fig. 4 Stress distributions at different expansion instants

Fig. 5 Pressure-expansion curves during continuous expansions with different a_0

Fig. 6 Size-dependent pressure-expansion curves with different values of ρ

Fig. 7 Comparison of limit expansion pressures with varying values of d_{50} / a

Fig. 8 Comparison of limit expansion pressures with varying values of ρ

Fig. 9 Variation of limit expansion pressure with typical values of a/d_{50}

Fig. 10 Variation of limit expansion pressure with typical values of G/p_0: (a) $\psi = 0^o$; (b) $\psi = 10^o$;(c) $\psi = 20^o$

Fig. 11 Comparison of pressure-expansion responses at small deformation levels

Fig. 12 Influence of the elastic strain rates in the plastic zone on the size-dependent pressure-expansion curves

Figures

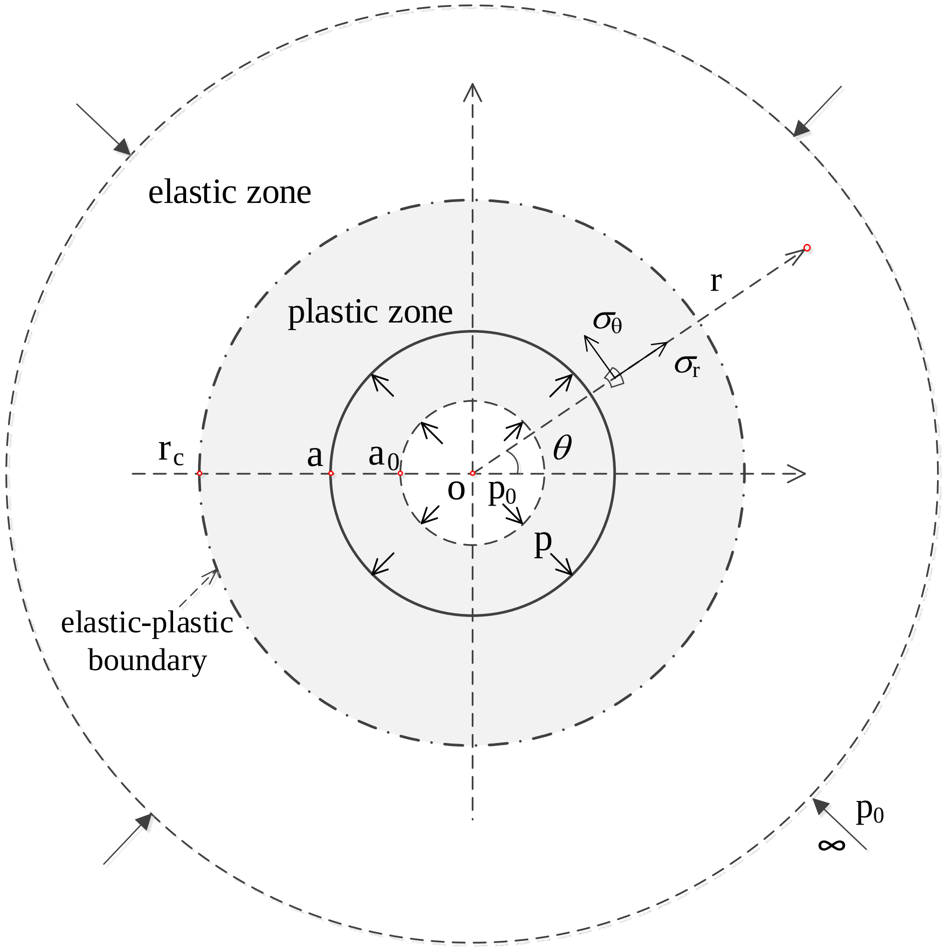

Fig. 13 Example boundary conditions during expansions of a cylindrical cavity

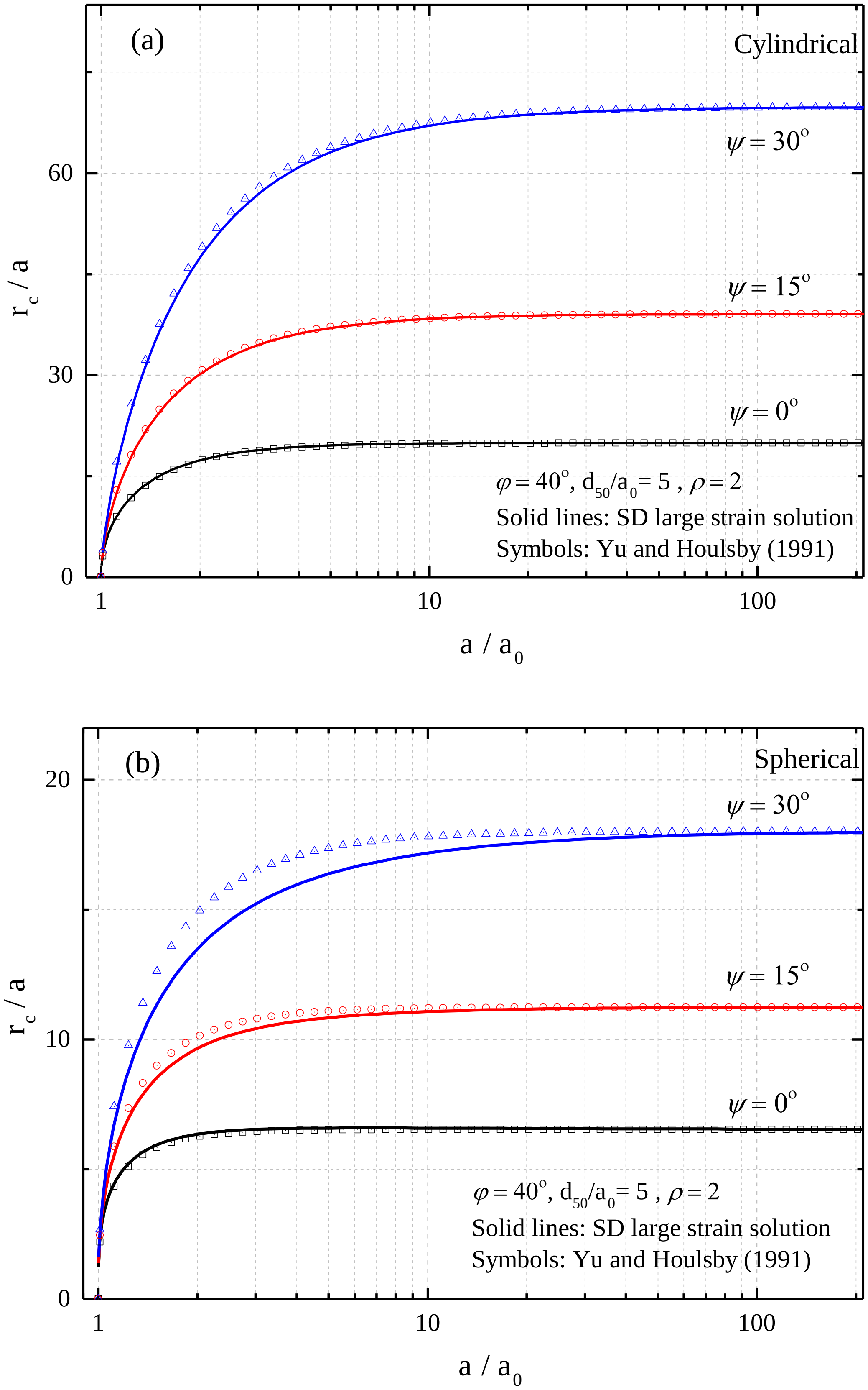

Fig. 14 Propagation of elastic-plastic boundaries during expansions ($p_0 = 50\text{kPa}$, $G / p_0 = 350$, $\varphi = 40^o$, $\psi = 15^o$, $\nu = 0.3$, $d_{50} = 1\text{mm}$)

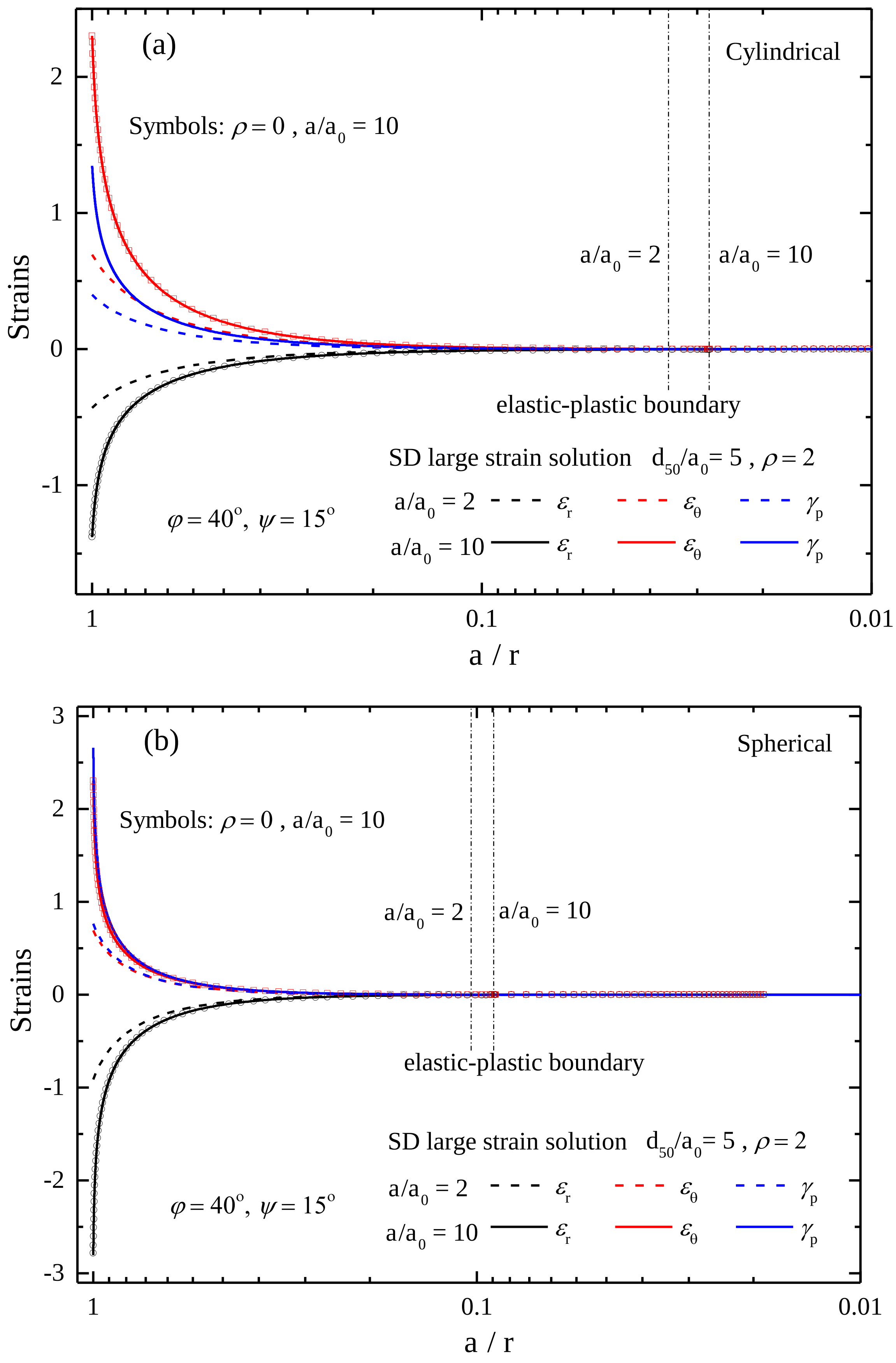

Fig. 15 Strain distributions at different expansion instants

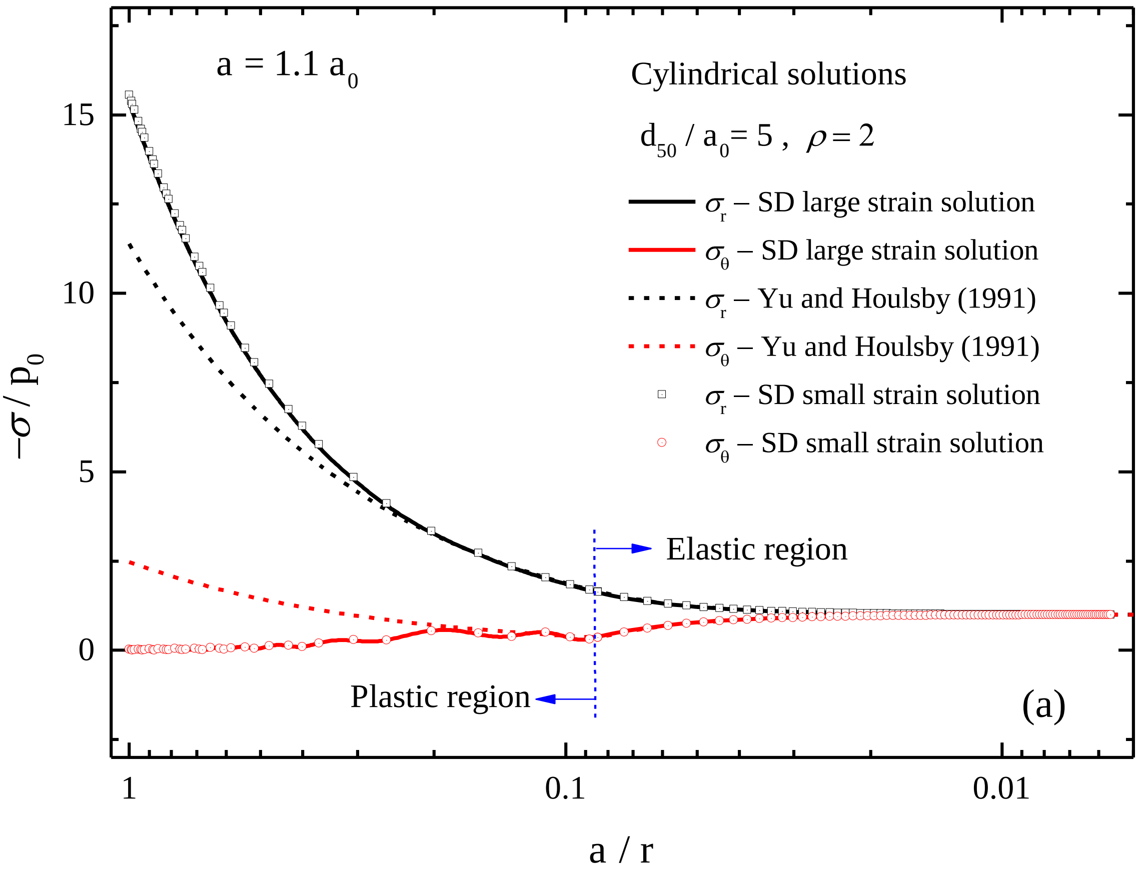
a = 1.1 a0
Cylindrical solutions
d50 / a0 = 5 , ρ = 2
σr – SD large strain solution
σθ – SD large strain solution
σr – Yu and Houlsby (1991)
σθ – Yu and Houlsby (1991)
σr – SD small strain solution
σθ – SD small strain solution
Elastic region
Plastic region
(a)
−σ / p0
a / r
15
10
5
0
1
0.1
0.01

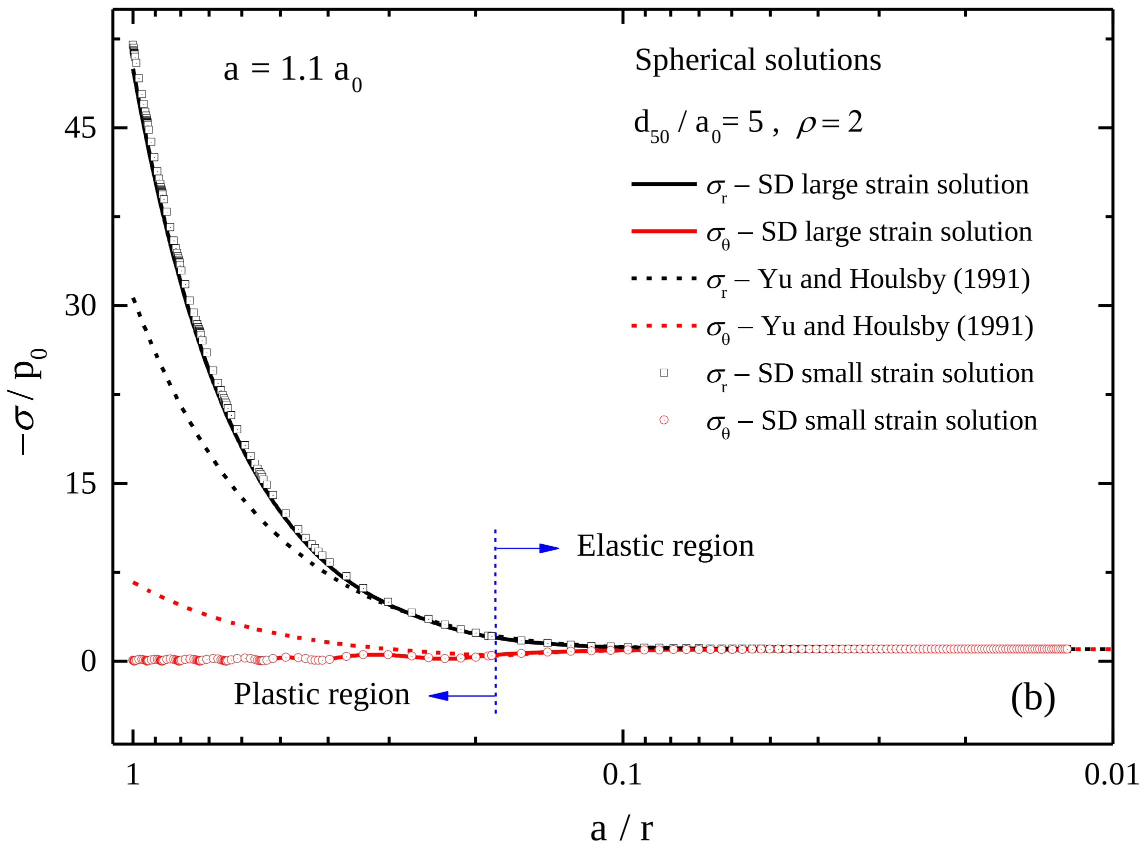
a = 1.1 a0
Spherical solutions
d50 / a0 = 5 , ρ = 2
σr – SD large strain solution
σθ – SD large strain solution
σr – Yu and Houlsby (1991)
σθ – Yu and Houlsby (1991)
σr – SD small strain solution
σθ – SD small strain solution
Elastic region
Plastic region
(b)
−σ / p0
a / r
45
30
15
0
1
0.1
0.01

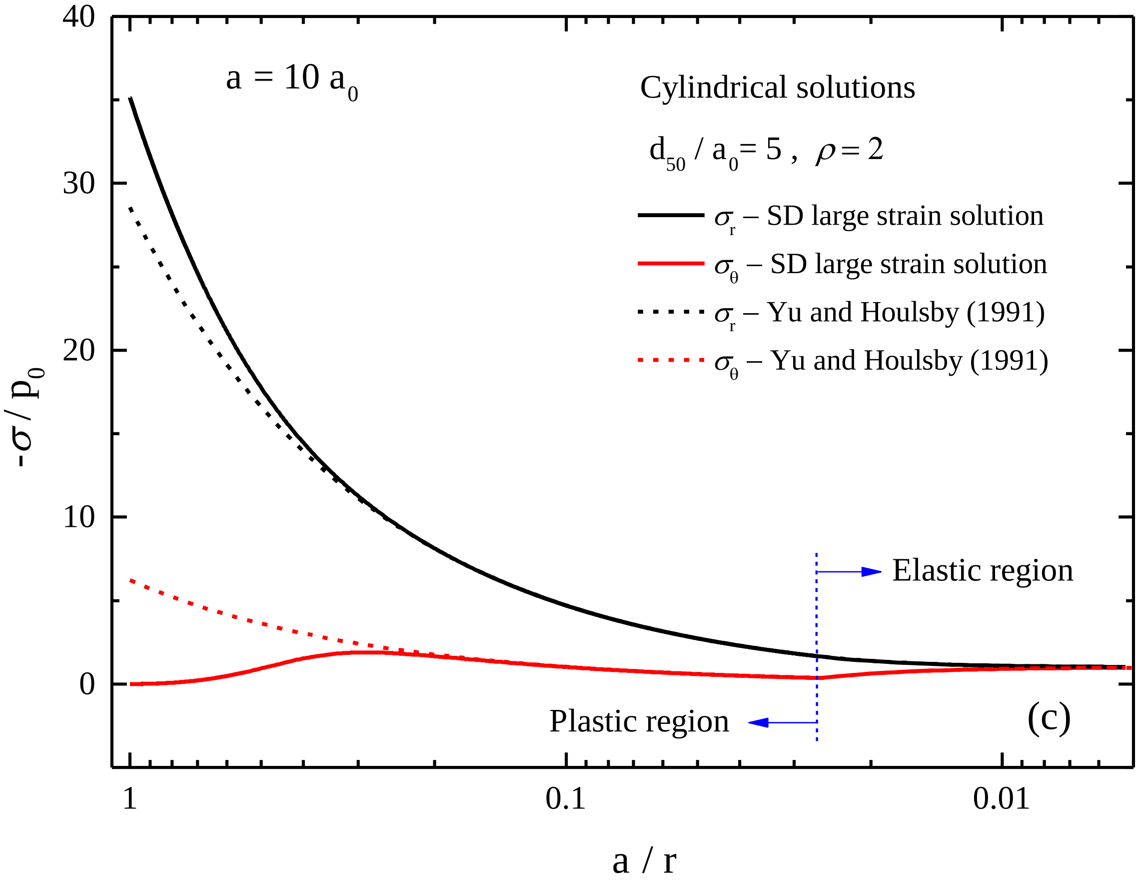

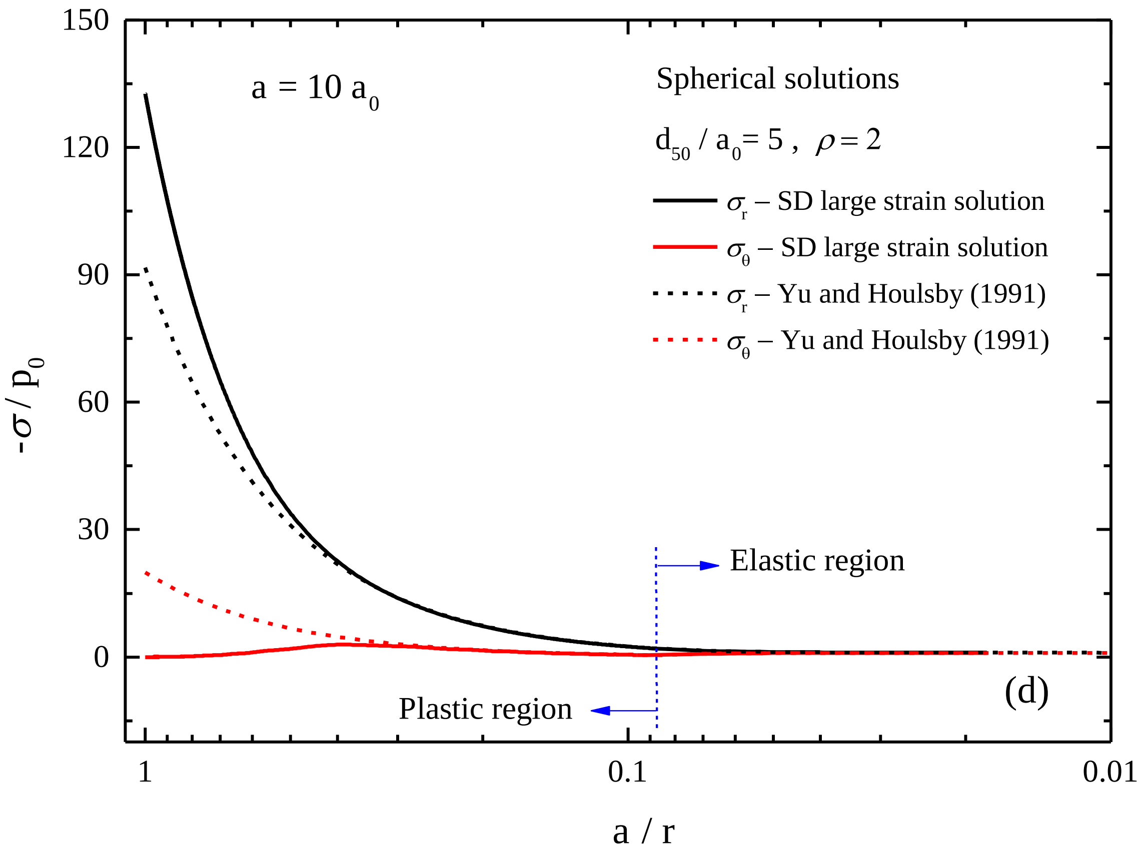

Fig. 16 Stress distributions at different expansion instants

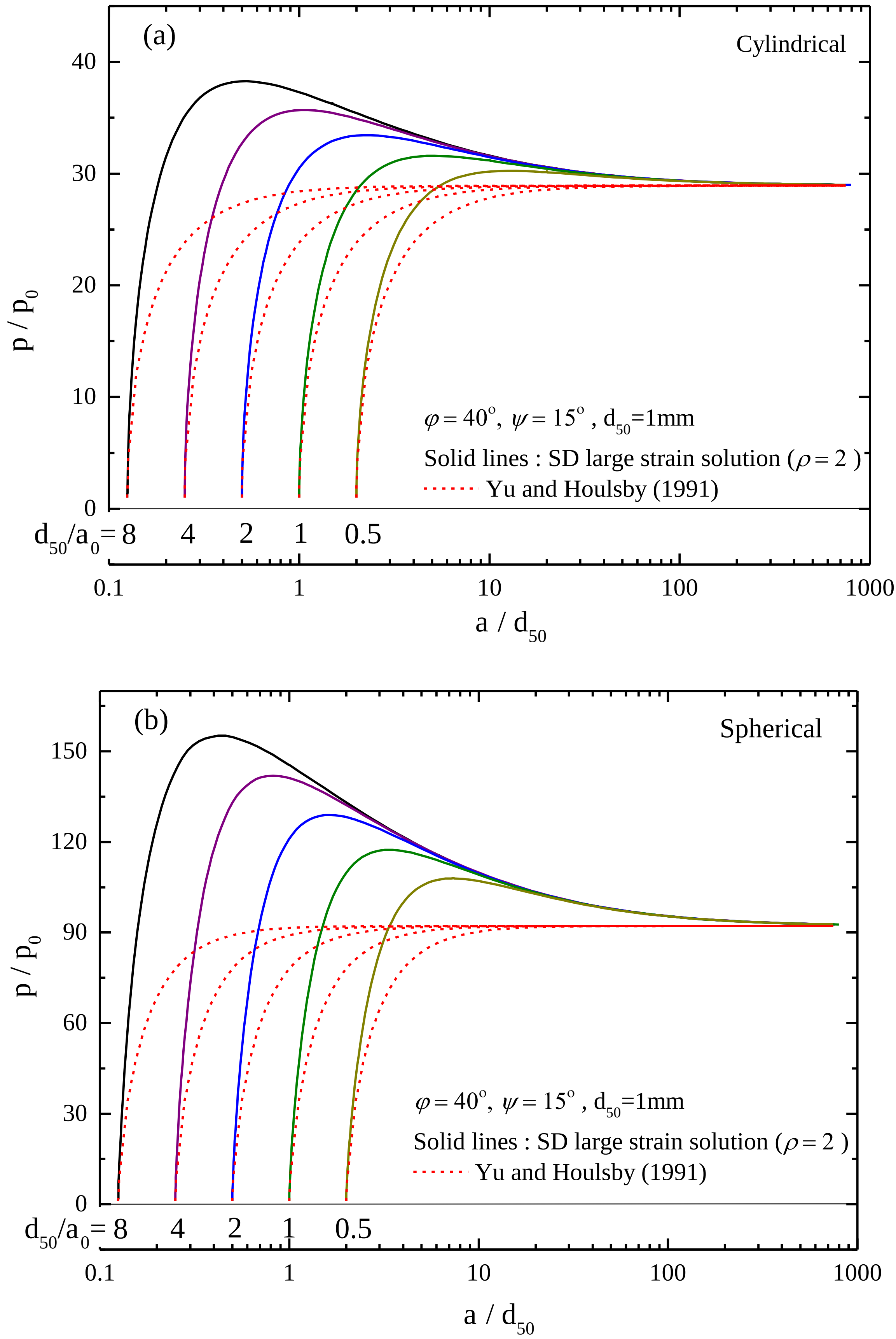

Fig. 17 Pressure-expansion curves during continuous expansions with different a_0

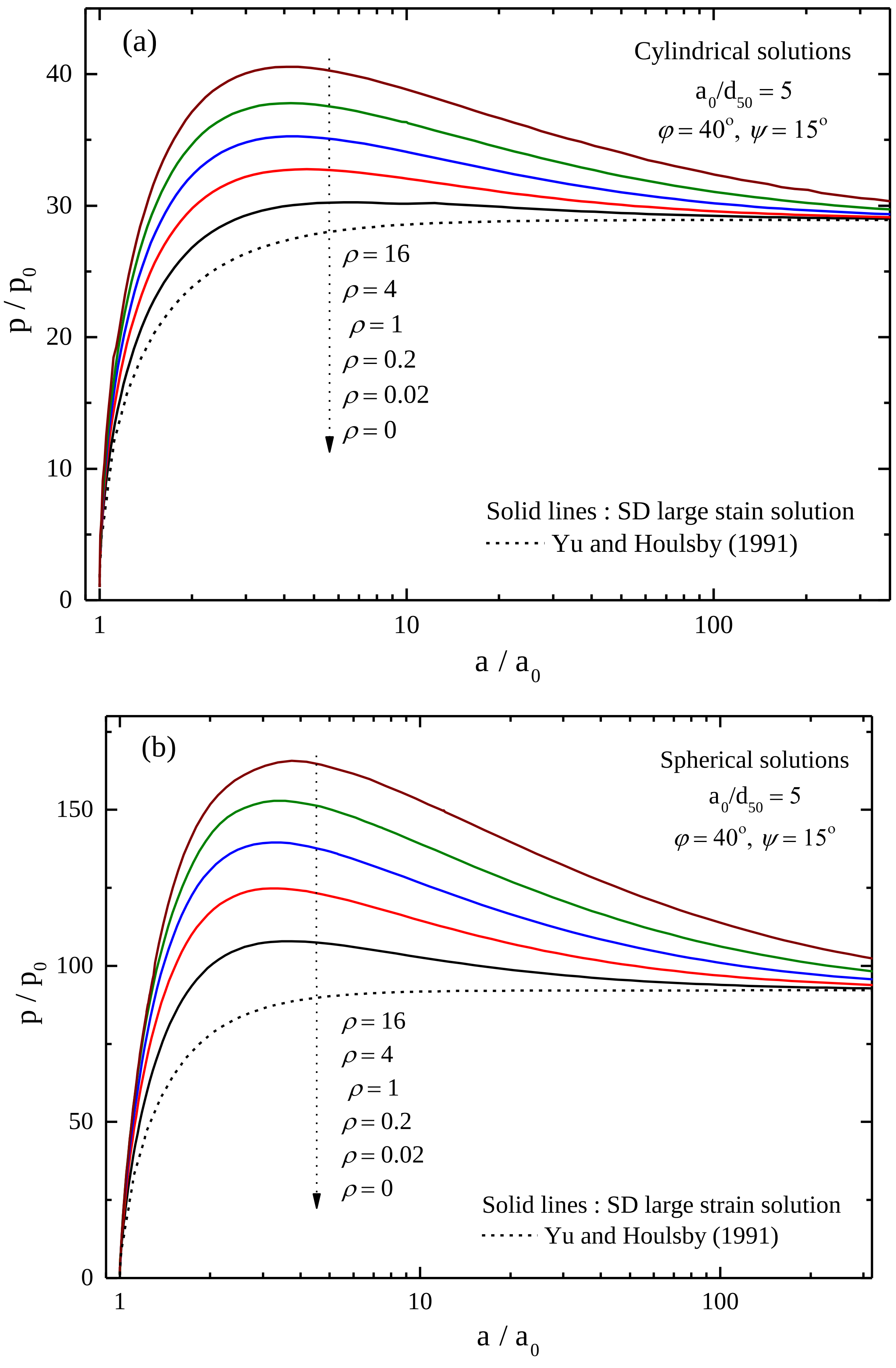

Fig. 18 Typical size-dependent pressure-expansion curves with different values of ρ

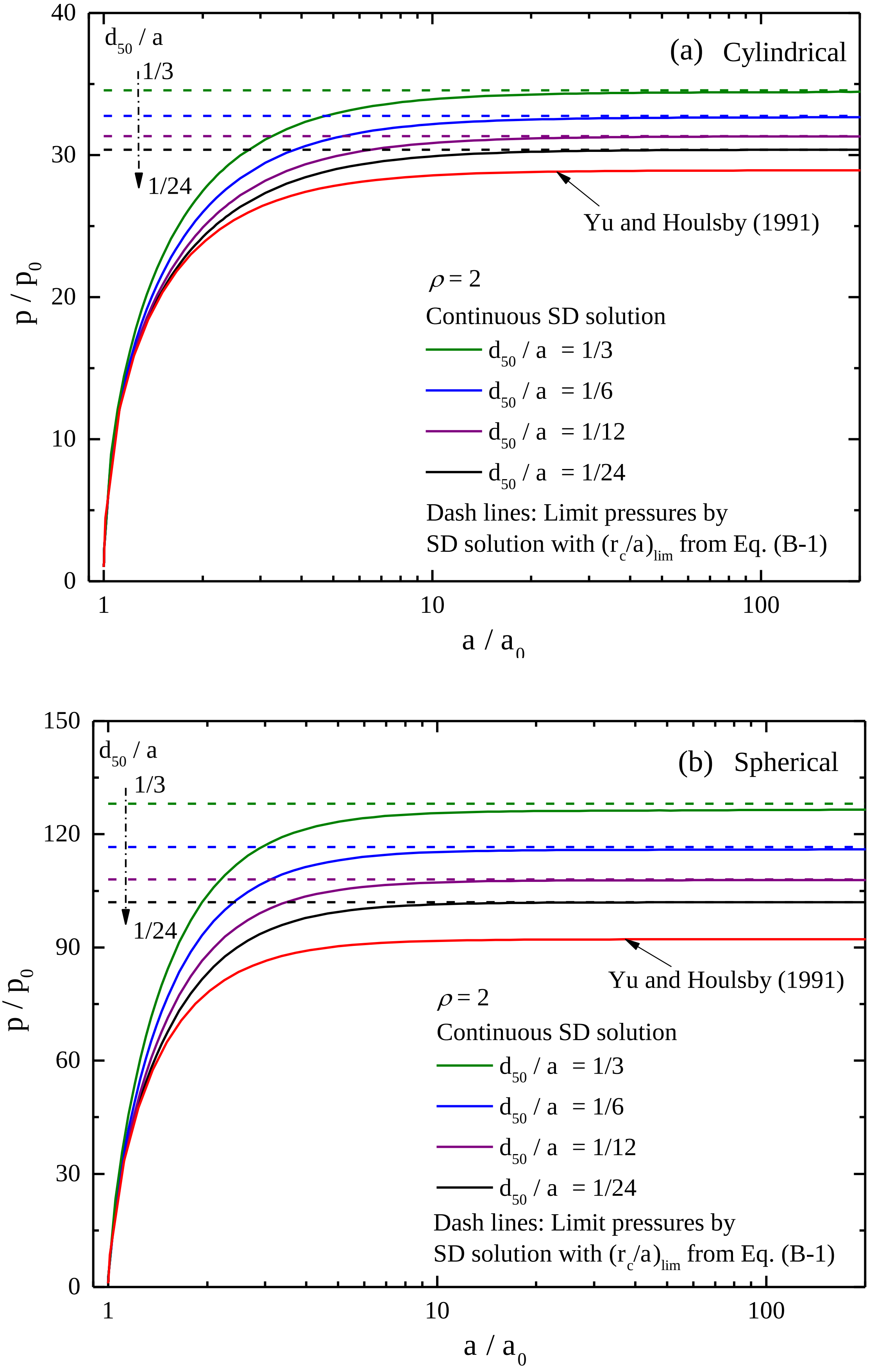

Fig. 19 Comparison of limit expansion pressures with varying values of d_{50} / a

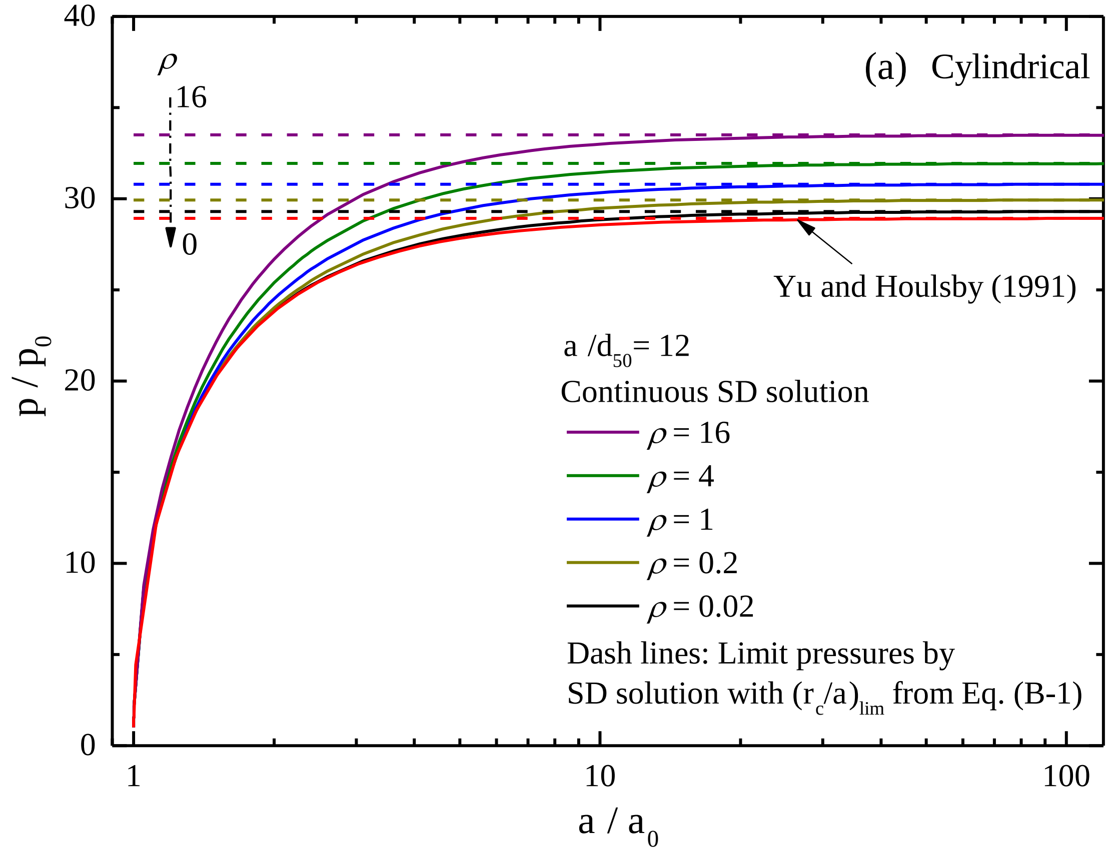

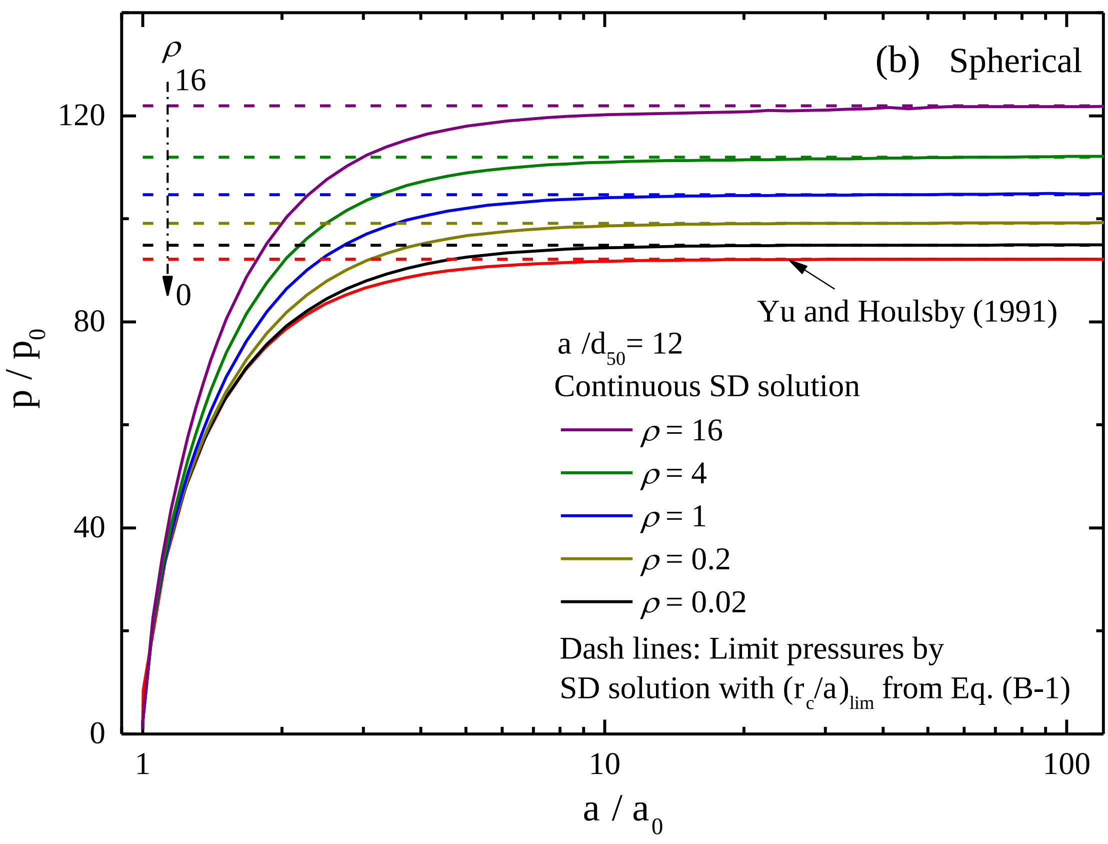

Fig. 20 Comparison of limit expansion pressures with varying values of ρ

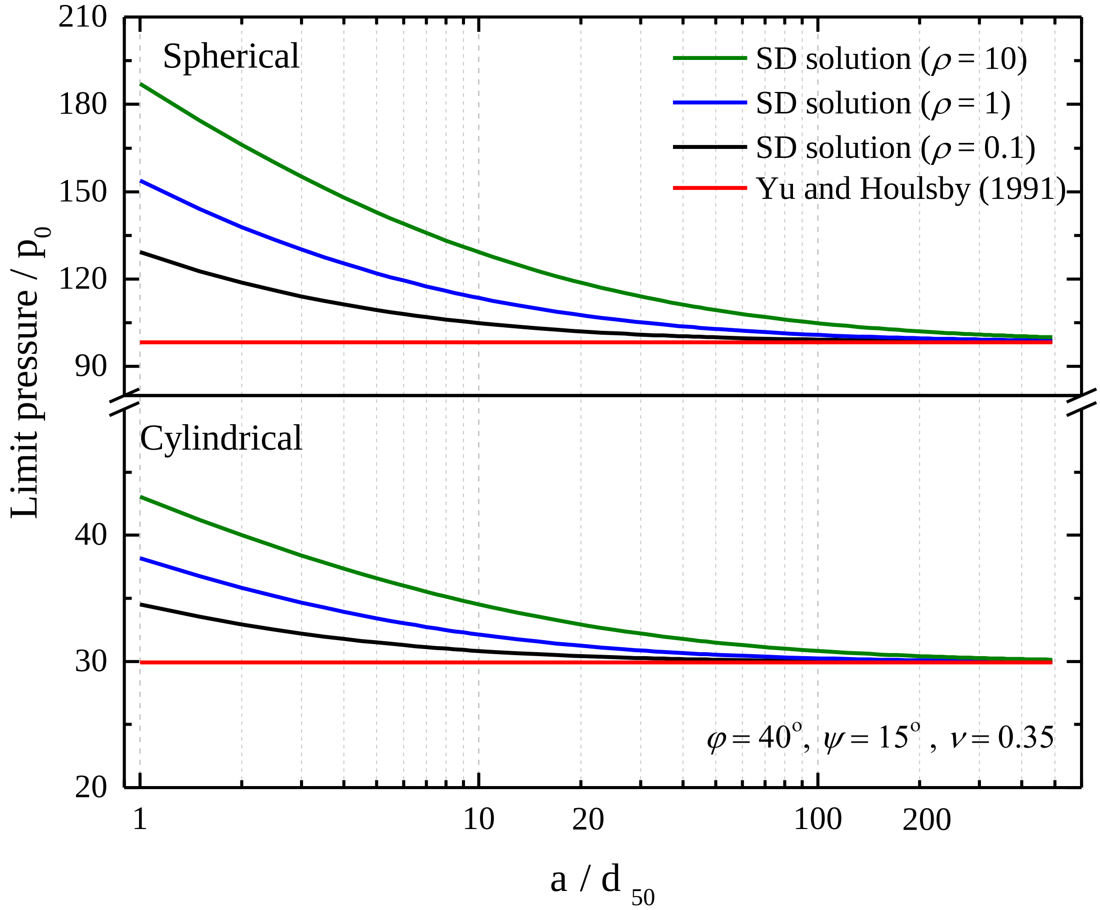

Fig. 21 Variation of limit expansion pressure with typical values of a/d_{50}

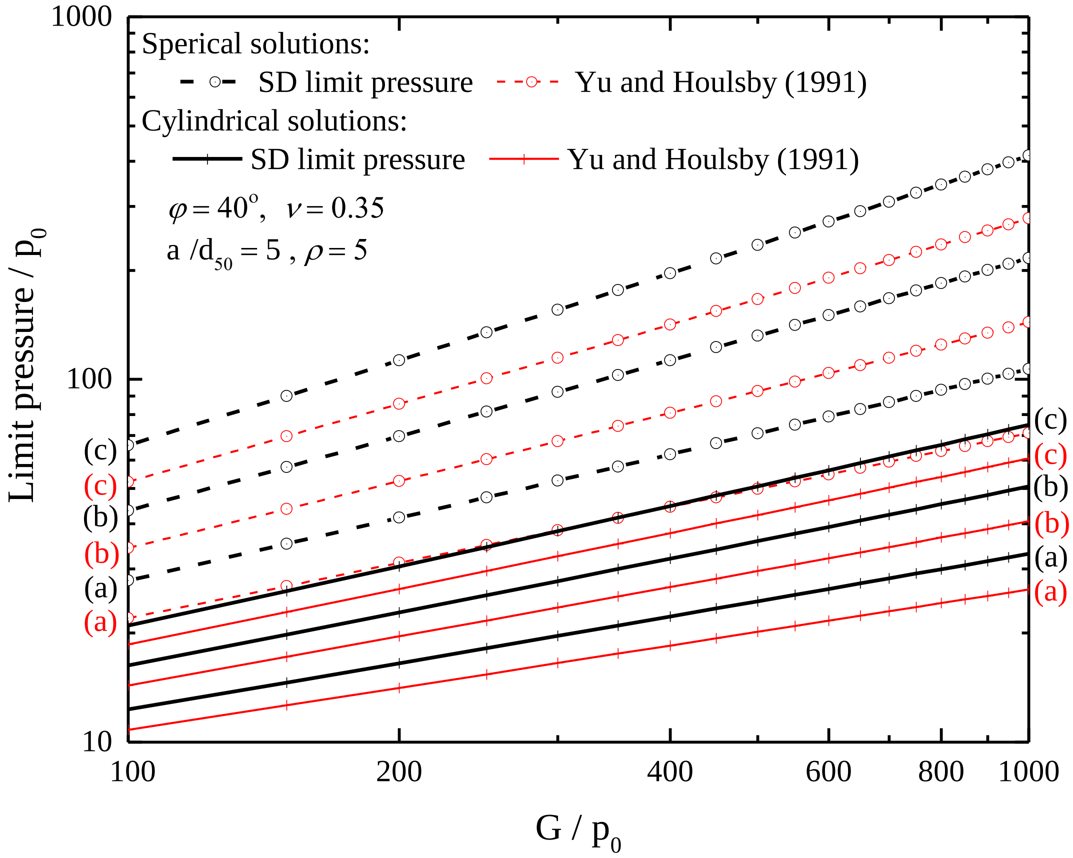

Fig. 22 Variation of limit expansion pressure with typical values of G/p_0: (a) $\psi = 0^{o}$; (b) $\psi = 10^{o}$; (c) $\psi = 20^{o}$

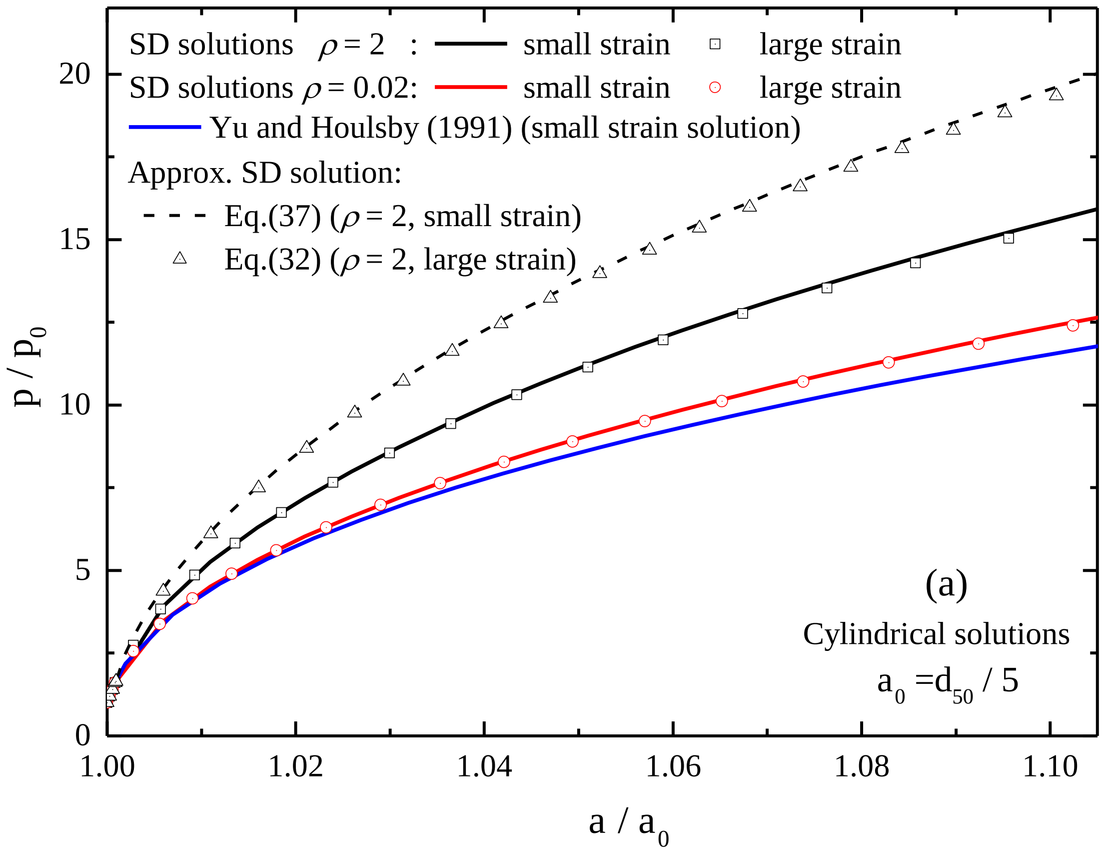

808

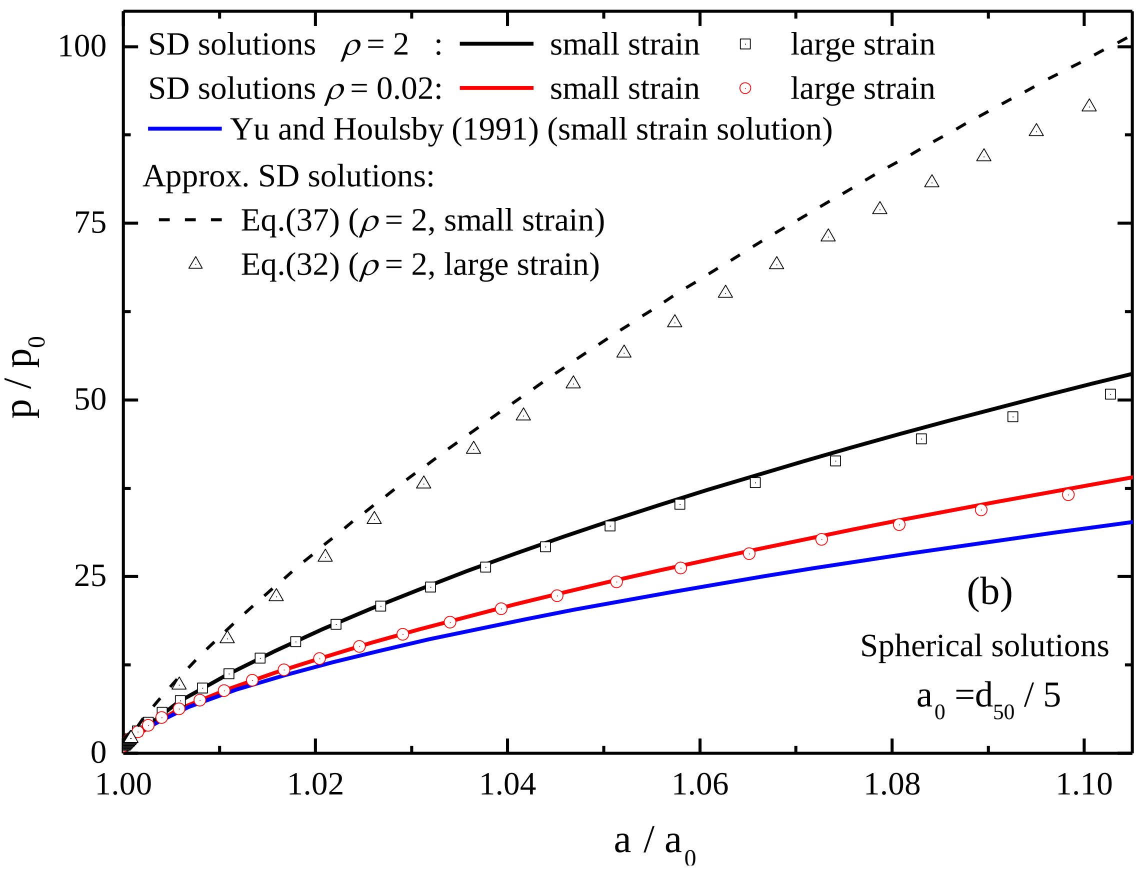

809

810 Fig. 23 Comparison of pressure-expansion responses at small deformation levels

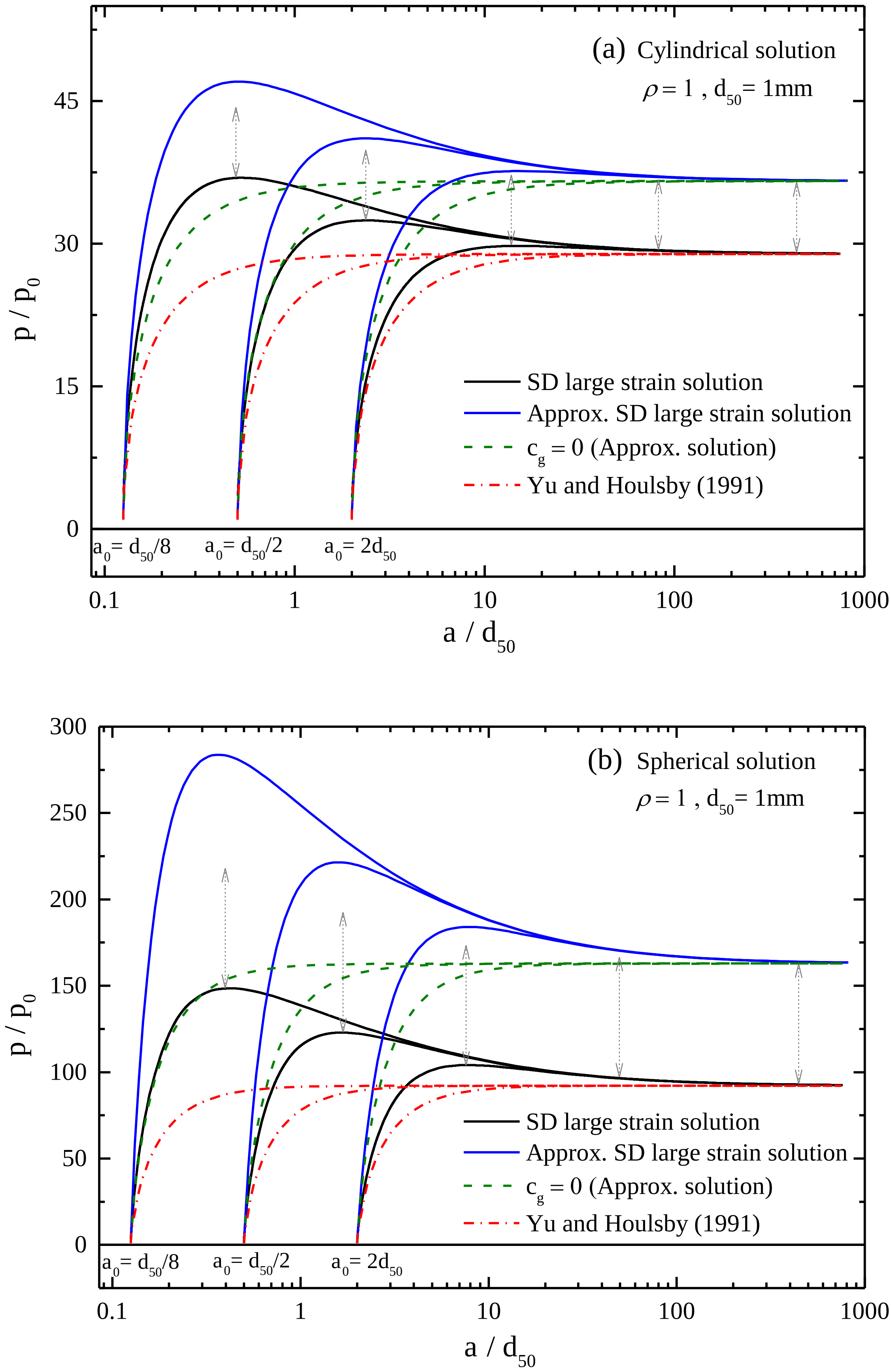

Fig. 24 Influence of the elastic strain rates in the plastic zone on the size-dependent pressure-expansion curves